Contrib Mineral Petrol (2004) 148: 335–357
DOI 10.1007/s00410-004-0607-x

ORIGINAL PAPER

Vladica Cvetković · Hilary Downes · Dejan Prelević
Milivoje Jovanović · Marina Lazarov

Characteristics of the lithospheric mantle beneath East Serbia inferred from ultramafic xenoliths in Palaeogene basanites

Received: 25 November 2003 / Accepted: 8 July 2004 / Published online: 12 August 2004

Abstract Mantle xenoliths from Paleogene basanites of East Serbia were studied using EMP and LA-ICP-MS techniques in order to better understand mantle characteristics in this region. Five different mantle lithologies have been distinguished: a dunite/harzburgite/lherzolite (D/HZ/L) group, clinopyroxene-rich lherzolites (Cpx-L), clinopyroxene megacrysts (Cpx-M), spinel-rich olivine websterites (OWB_1) and spinel-poor olivine websterites (OWB_2). D/HZ/L xenoliths are the most common and represent 'normal' mantle composed of typical anhydrous spinel peridotites with well equilibrated, unzoned silicates characterized by high Mg# s. Negative correlations between Mg# and TiO_2, Al_2O_3 and CaO wt% in clinopyroxenes (cpx) and orthopyroxenes (opx) and the Cr–Al trend in spinel (sp) suggest depletion via extraction of basaltic melts. The modal composition of D/HZ/L xenoliths and unusual low-Al opx suggest that the lithospheric mantle underneath East Serbia is more depleted than normal European lithosphere. D/HZ/L xenoliths contain numerous pockets and veins filled by Cr-rich cpx, Ti-rich spinel, altered glass, apatite and rare ilmenite and phlogopite. Petrographic observations, supported by major element contents in sp and cpx, and modelling using trace element contents in cpx, indicate that the pockets and veins formed from infiltration of alkaline melts and reaction with peridotite wall-rock causing opx and spinel replacement. The same alkaline melt-related metasomatism gave rise to the Cpx-L and OWB_1 mantle xenoliths and Cpx-M xenocrysts. Trace element contents of cpx in these xenoliths show a distinctively concave downwards REE pattern with a HFSE depletion, very similar to cpx megacrysts from the Pannonian Basin and to vein cpx from Eifel. In contrast, the OWB_2 xenoliths show evidence of precipitation from subduction-related mafic to ultramafic melts, as inferred from their opx-rich lithology and unusual Cr-rich spinels. They are probably related to subduction magmatism during the Late Cretaceous.

Milivoje Jovanović: deceased in April 2004

Editorial Responsibility: T. L. Grove

V. Cvetković (✉) · D. Prelević
Faculty of Mining and Geology, University of Belgrade,
Đušina 7, 11000 Belgrade, Serbia and Montenegro
E-mail: cvladica@mkpg.rgf.bg.ac.yu

H. Downes
Research School of Earth Sciences,
Birkbeck College, Malet St., London, WC1E 7HX UK

M. Jovanović
Institute for Stone and Aggregates,
11000 Belgrade, Serbia and Montenegro

M. Lazarov
Institute für Mineralogie, Johann Wolfgang Goethe-Universität,
Senckenberganlage 28, 60054 Frankfurt am Main, Germany

Introduction

Ultramafic xenoliths in alkali basalts provide important information concerning the mineralogy and geochemistry of the subcontinental lithospheric mantle (e.g. Frey and Green 1974; Mercier and Nicholas 1975; Wilshire and Pike 1975; Wilshire and Shervais 1975; Frey and Prinz 1978; Menzies 1983; Nicolas et al. 1987; Griffin et al. 1998). Major mantle processes such as depletion and enrichment can be investigated via the study of textural relations and mineral compositions in such xenoliths (e.g. Amundsen et al. 1987; O'Reilly 1989; Grégoire et al. 1997; Xu et al. 1998; Griffin et al. 1999; Dawson 2002). Mantle xenoliths found in Tertiary/Quaternary alkali basalts have been extensively studied in many parts of Europe (see review by Downes 2001). Although mantle xenoliths were thoroughly studied across the Pannonian Basin (e.g. Downes et al. 1992; Embey-Isztin et al. 1989, 2001; Szabó et al. 1995, etc.), information about the lithosphere beneath south-east Europe, especially the Balkan Peninsula, is very scarce. Jovanović et al. (2001) and Cvetković et al. (2001) presented the first information on xenoliths from East

Serbia and discussed mantle processes within the lithosphere beneath the Balkans. These studies are reported in more detail in this paper.

We have investigated upper mantle xenoliths hosted in Palaeogene basanites of Serbia. We present textural evidence and mineral chemistry data on a variety of ultramafic xenoliths in order to determine the dominant characteristics of the mantle lithosphere beneath the region and to shed light on the processes that controlled the observed mineralogical trends. Laser ablation-inductively coupled plasma-mass spectrometer (LA-ICP-MS) trace element data of clinopyroxenes (cpx) from a subset of these xenoliths are also discussed, in order to better understand metasomatic processes that occurred within the East Serbian lithosphere.

We demonstrate that the mantle beneath this part of the Balkans is dominantly harzburgitic and records ancient depletion events involving the extraction of basaltic melts, and later metasomatism via introduction of alkaline mafic melts. Thermometric calculations and pressure estimates suggest that heat-flow in East Serbia at the beginning of Cainozoic times was lower than in the adjacent Pannonian area (e.g. Lankreijer et al. 1997), in keeping with a lack of subsidence in the Balkans. We also highlight a specific sub-group of olivine websterite xenoliths and relate them to percolation and consolidation of subduction-related magmas.

Regional setting and host rocks

Late Cretaceous and Palaeogene geodynamics of the Balkan Peninsula were related to subduction followed by syn-collisional and post-collisional/relaxation tectonics. In a more general context this was related to the final closure of the Tethyan Ocean, when the present terrane framework was established (Fig. 1A). This gave rise to several separate periods of mantle-derived magmatism (Cvetković et al. 2004). Mafic alkaline rocks in East Serbia are Palaeogene in age and form a north-south line within the Carpatho-Balkan tectonic terrane, parallel to the arc/fore-arc region of the presumed Cretaceous subduction zone (Ianovici et al. 1977; Karamata et al. 1997). Jovanović et al. (2001) presented petrological and geochemical data for these rocks and showed an age range from 62 to 39 Ma. Alkaline rocks occurring further north in Poiana Rusca (Romania) represent the northern continuation of the same volcanic chain. Reporting petrography and geochemistry of alkaline rocks of this locality Downes et al. (1995) presented some initial data on mantle xenoliths. Similar mantle xenolith-bearing rocks occur in Bulgaria (Marchev et al. 1997; Vaselli et al. 1997) but they are clearly related to younger tectonic events. They crosscut the Moesian platform in a N–S direction and are Upper Oligocene to Lower Miocene in age.

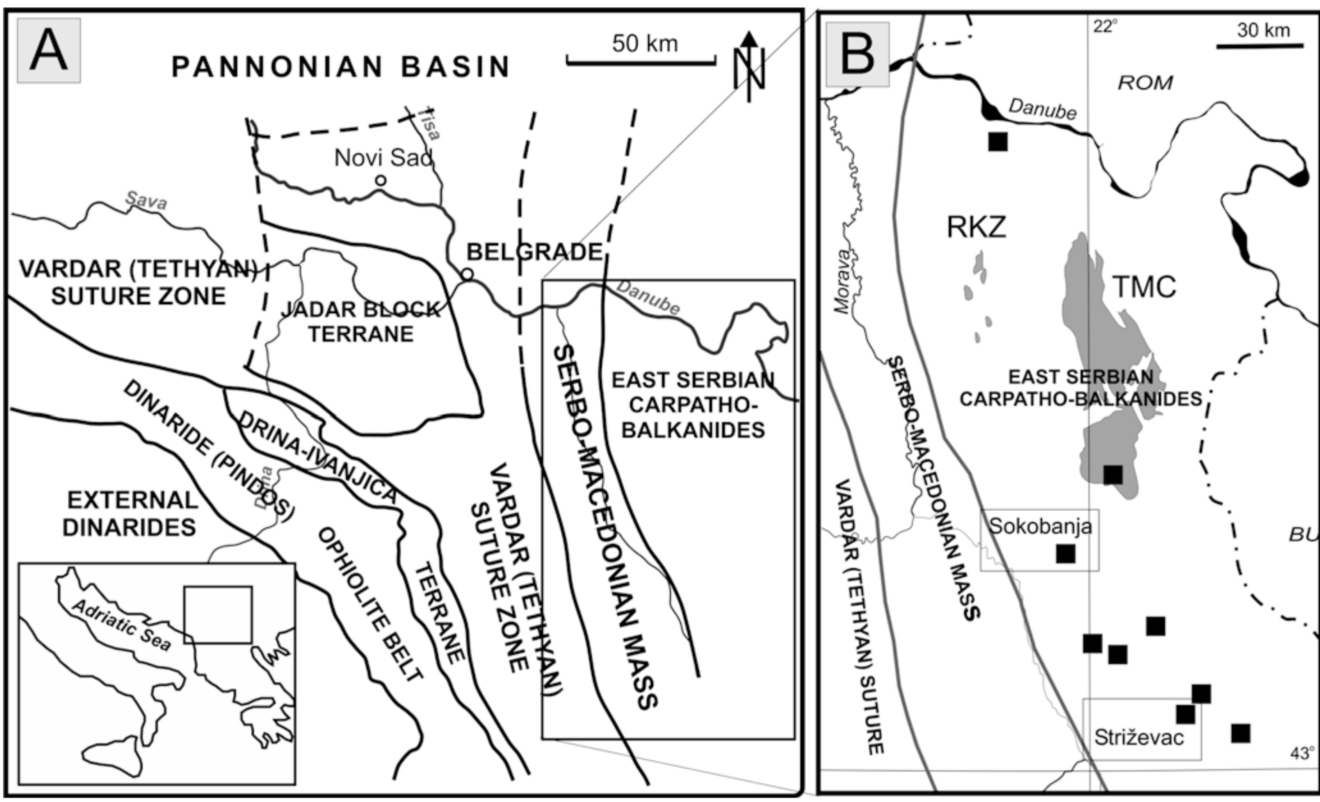

Fig. 1A,B **A** Geotectonic sketch of the central Balkan Peninsula (Karamata et al. 1994), **B** distribution of East Serbian Palaeogene mafic alkaline rocks (*full squares*). The locations of mantle xenolith-bearing alkaline rocks are shown in squares and the distribution of Late Cretaceous volcanic rocks of the Ridanj-Krepoljin Zone (*RKZ*) and Timok Magmatic Complex (*TMC*) is also presented

The alkaline magmatism of East Serbia post-dates the Late Cretaceous subduction-related magmatism, for which high precision U–Pb age determinations have yielded ages from 86 to 70 Ma (von Quadt et al. 2003), i.e. they are at least 10 m.y. older than the Palaeogene alkaline rocks. Mantle xenolith-bearing East Serbian mafic alkaline rocks occur as small and rare relicts of lava flows and volcaniclastics. They are porphyritic rocks with olivine and clinopyroxene as main phenocrysts. Jovanović et al. (2001) and Cvetković et al. (2004) showed that the petrogenesis of the Palaeogene alkaline rocks does not require any subduction component. These rocks are silica-undersaturated with high Nb contents, low LILE/HFSE ratios and depleted isotopic signatures. The spatial distribution of mantle xenolith-bearing alkaline rocks in Serbia and their relation to the earlier subduction-related magmatism (Ridanj-Krepoljin zone and Timok magmatic complex) is shown in Fig. 1B.

Petrography and classification of mantle xenoliths

Ultramafic xenoliths and clinopyroxene megacrysts (Cpx-M) have been found at two localities in the East Serbian alkaline volcanic area—Sokobanja in the north and Striževac around 100 km further south (Fig. 1B). Thirty-five samples have been investigated. The xenoliths are fairly small, ranging from around 10 cm to a few millimetres. The largest xenoliths usually are totally altered. When fresh, they appear as yellow-green, green to dark-green rounded to subrounded patches enclosed by a black basanitic host. Clinopyroxene phenocrysts appear as mostly fresh black angular to subrounded fragments ranging in size from 5 cm to <1 mm. Only totally fresh xenoliths and xenocrysts were sampled.

Modal analyses of the xenoliths (around 50% of the total sample area) were performed using scanned thin-section images. The scanned images were digitised manually and then the total surface for appropriate minerals was computed using 3D software. The results are shown in Table 1. This method has been proved to give better reproducibility (less than 5%) than conventional point-counting. The minerals present in negligible amounts (pocket and veinlet assemblages) were disregarded during the modal analysis. However, pockets with >50 vol% clinopyroxene were counted as cpx. Within the dunite/harzburgite/lherzolite thin-sections (D/HZ/L—see below), we distinguish "primary" mineral associations, typical of four-phase anhydrous mantle peri-

Table 1 Modal analyses, classification and texture of mantle xenoliths found in East Serbian Palaeogene mafic alkaline rocks

No.	Ol (vol%)	Opx	Cpx	Spl	Classification
Sokobanja					
X-1	59.0	9.5	28.7	2.8	Cpx-L, protogranular, undeformed
X-4	6.8	0.0	93.2	0.0	Cpx-M, undeformed
X-5	98.1	0.0	1.8	0.0	Spinel-free dunite, slightly deformed
X-6	88.4	9.7	1.6	0.3	Harzburgite, protogranular, undeformed
X-9S	77.8	17.7	4.5	0.0	Harzburgite, protogranular, undeformed
X-10	20.0	0.0	82.0	0.0	Ol-bearing clinopyroxene megacryst, undeformed
X-11/1	59.6	22.2	17.1	1.1	Cpx-L, protogranular, undeformed
X-11/2	71.1	20.1	7.2	1.7	Lherzolite, protogranular, slightly sheared
X-13	99.0	0.0	0.0	1.0	Spinel-free dunite, slightly deformed
K-8	0.0	0.0	100.0	0.0	Cpx-M, undeformed
K-13	82.0	13.0	3.7	1.1	Harzburgite, protogranular, slightly sheared
K-19	67.7	25.2	5.1	2.0	Harzburgite, protogranular, slightly sheared
SB-3	6.6	73.5	17.6	2.3	OWB_1, protogranular, undeformed
SB-4	46.1	45.7	5.4	2.8	Lherzolite, protogranular, undeformed
X-20-1	28.3	62.0	9.7	0.0	OWB_2, slightly deformed
X-20-1a	43.9	49.4	5.9	0.8	Lherzolite, protogranular, undeformed
X-20-2	72.3	10.6	16.1	1.0	Cpx-L, protogranular, undeformed
X-20-3	90.2	0.0	7.7	3.1	Spinel-bearing dunite, protogranular, undeformed
X-20-5	10.6	66.6	20.2	2.5	OWB_1, protogranular, undeformed
X-20-6	20.1	75.4	4.5	0.0	OWB_2, slightly deformed
X-20-7	70.0	22.1	6.0	2.4	Lherzolite, protogranular, undeformed
X-20-9	15.0	75.0	9.5	0.5	OWB_2, slightly deformed
X-20-10	19.5	68.2	8.5	3.8	OWB_1, protogranular, undeformed
X-20-11	9.2	80.1	10.7	0.0	OWB_2, slightly deformed
X-20-15	70.1	20.5	8.1	1.3	Harzburgite, protogranular, undeformed
Striževac					
Stz-20-1	63.5	29.9	6.1	0.5	Lherzolite, protogranular, slightly sheared
Stz-20-2	72.5	16.8	9.2	1.5	Lherzolite, protogranular, undeformed
Stz-20-3	68.8	30.0	0.5	0.7	Harzburgite, protogranular, slightly sheared
Stz-20-4	72.8	23.3	3.2	0.7	Harzburgite, protogranular, undeformed
Stz-20-6	97.5	0.0	0.0	2.5	Spinel-bearing dunite, protogranular, undeformed
Stz-20-7	80.6	12.4	5.1	1.9	Lherzolite, protogranular, slightly deformed
Stz-20-9	85.2	11.9	2.3	0.7	Harzburgite, protogranular, undeformed
Stz-20-11	86.0	10.5	2.2	1.3	Harzburgite, protogranular, undeformed
Stz-20-12	72.3	24.2	3.2	0.4	Harzburgite, protogranular, slightly deformed

dotites, and "secondary" minerals that are often present in small amounts in pockets and veinlets and are believed to be the result of metasomatic processes.

The Ol-Opx–Cpx classification diagram (Streckeisen 1973) for East Serbian xenoliths is shown in Fig. 2. The fields of modal composition of spinel peridotite xenoliths from Poiana Rusca (Downes et al. 1995) and Ray Pic (French Massif Central) (Zangana 1995) are also presented in order to compare Serbian xenoliths with a non-metasomatised, normal mantle lithology. Several different groups can be distinguished. Most Serbian xenoliths plot in the olivine-rich section of the diagram, encompassing D/HZ/L types. This group has modal compositions similar to upper mantle xenoliths from Poiana Rusca as well as to mantle-derived spinel peridotites worldwide and will be referred to as the D/HZ/L group. The East Serbian D/HZ/L xenoliths are largely confined to the harzburgite field and the area very close to the HZ/L boundary. Three samples (X-1, X-11/1 and X-20-2) contain significantly more clinopyroxene than normal lherzolites. They are regarded as a sub-group which we term clinopyroxene-rich lherzolite (Cpx-L).

A significant number of East Serbian xenoliths plot in the olivine websterite field and will be referred to as the OWB samples. These unusual lithologies contain > 60 vol% orthopyroxene with variable proportions of olivine and clinopyroxene (Table 1).

Dunite/Harzburgite/Lherzolite (D/HZ/L) and clinopyroxene-rich (Cpx-L) xenoliths

These are mostly rounded to subrounded xenoliths, some of which are slightly elongated and may show

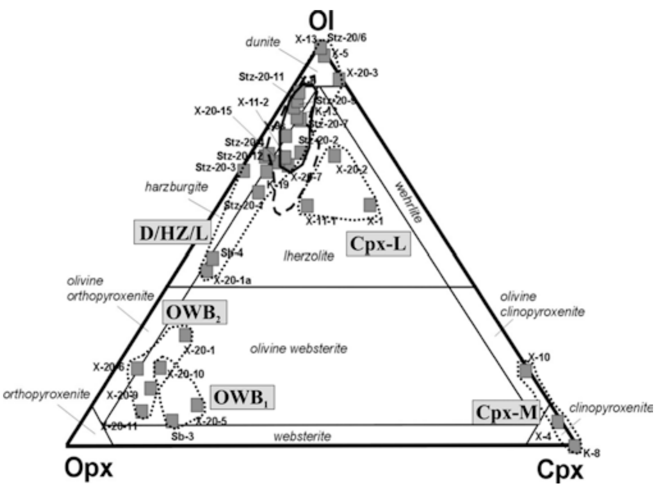

Fig. 2 Opx–Cpx-Ol classification diagram (Streckeisen et al. 1973) showing modal composition of East Serbian xenoliths (*gray squares*); major lithologies are outlined and abbreviated as follows: *D/HZ/L* dunite/harzburgite/lherzolite, *Cpx-L* clinopyroxene-rich lherzolite, OWB_1 spinel-rich olivine websterite, OWB_2 spinel-poor olivine websterite and *Cpx-M* clinopyroxene megacrysts; modal composition of Poiana Rusca (Downes et al. 1995) (*full line*) and Ray Pic spinel peridotite xenoliths (Massif Central; Zangana 1995) (*dashed line*) are also shown

shearing. They range from 10 to < 0.5 cm in diameter. Contacts between the xenoliths and the surrounding basaltic groundmass are sharp but usually irregular. The xenoliths are anhydrous four-phase peridotites with olivine, orthopyroxene, clinopyroxene and spinel as the predominant constituents. All these minerals are essentially fresh, with serpentinisation only developed along cracks within olivine and some orthopyroxene crystals. They form curvilinear grain boundaries with very rare triple junctions. Most of the D/HZ/L xenoliths are undeformed and have protogranular textures (Fig. 3A). The predominant grain size is around 2×3 mm. Substantially larger olivine grains are characteristic for some dunites, while Cpx-L xenoliths are fine-grained with crystals often around 0.5 mm in diameter (Fig. 3B). Clinopyroxene is present in the form of clearly developed crystals only in the Cpx-L xenoliths but is essentially absent in harzburgite. Most frequently, clinopyroxene crystals are very small and observable only by BSE imaging. Spinel usually appears as small, equidimensional and isolated grains, but some samples contain irregular or patchy concentrations of spinel grains.

Besides the primary mantle mineralogy, the D/HZ/L xenoliths contain numerous milimetre-sized pockets and veinlets mainly containing clinopyroxene. Such pockets are usually rounded to subrounded or slightly elongated and are often fed by veinlets around 50 μm thick (Fig. 3B). These veinlets differ from the veins cutting through the whole xenoliths (Fig. 3C) in that the latter are thicker, they do not feed but cut some pockets, they contain nepheline and have a similar colour to the basanitic groundmass. When situated at the periphery of xenoliths, the pockets show sharp contacts with the enclosing basanite. Elongated pockets are commonly sub-parallel to the longer axis of xenoliths. Clinopyroxene is mostly euhedral, suggesting crystallization from the surrounding melt (Fig. 3D). Sometimes transitions appear from euhedral clinopyroxene-bearing stringers, through clinopyroxene-glass simplectites to coarser but spongy clinopyroxene crystals. Cpx within the pockets are green and clearly differ from the zoned, pale-pinkish cpx in the basanite groundmass. Clinopyroxene also occurs as a product of orthopyroxene replacement, forming overgrowths surrounding orthopyroxene relics within pocket assemblages (Fig. 3E). Similar orthopyroxene–clinopyroxene relationships were described by Xu et al. (1996). Sometimes patchy cpx occur around isolated orthopyroxene crystals with no apparent relation to pockets (Fig. 3F). The orthopyroxene replacements inside xenoliths are texturally different from those found at the contacts of orthopyroxene with basanitic magma in that the latter usually form characteristic selvages with tiny clinopyroxene and olivine crystals. They are oriented perpendicularly to the reaction surface (Fig. 3G). Apart from clinopyroxene, the pocket and veinlet assemblages are composed of severely altered glass, needles of apatite, Ti-rich spinel and rare olivine,

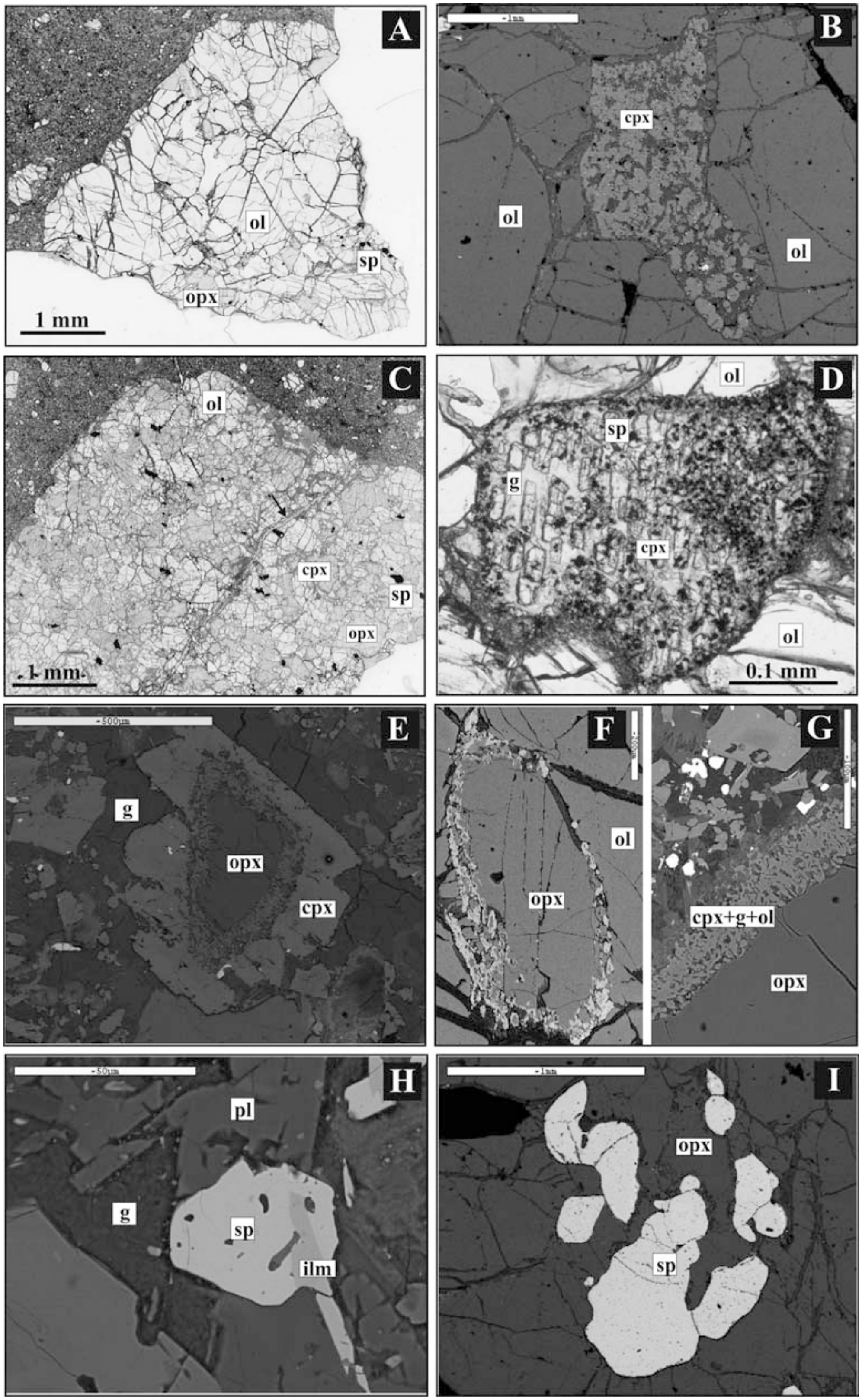

Fig. 3A–I **A** A plane-polarized light (*PPL*) scanned image of an undeformed protogranular harzburgite xenolith (X-6), **B** a back-scatter electron (*BSE*) image of a clinopyroxene-rich pocket surrounded by olivine grains and fed by tiny veinlets (X-11-2), **C** a PPL scanned image of a Cpx-L xenolith (X-11-1); the xenolith is cut by a host-related vein (*arrow*), **D** a PPL photomicrograph of a pocket containing subparallel oriented euhedral clinopyroxene, tiny grains of Ti-rich spinel and interstitial altered glass (stz 20-12), **E** a BSE image of a pocket containing clinopyroxene overgrowth around a relic of orthopyroxene; note outer euhedral faces of the clinopyroxene and simplectite contact with the opx relic; around the cpx very small Ti-rich spinels and interstitial dark glass may be observed (stz 20-12), **F** a BSE image of an isolated orthopyroxene crystal rimmed by patchy clinopyroxenes; the crystal is situated inside a xenolith (X-6, Fig. 3A), **G** BSE image of a clinopyroxene-olivine-glassy selvages found at the contact between peripheral orthopyroxene and basanitic groundmass (X-9s), **H** BSE image of a tiny Ti-rich spinel containing glassy blebs and one needle-shaped ilmenite crystal (stz 20-3), **I** BSE image of a disintegrated spinel grain transformed to a jig-saw fit puzzle of smaller and irregular spinel relics (X-11-2); Abbreviations: *ol* olivine, *opx* orthopyroxene, *cpx* clinopyroxene, *sp* spinel, *g* glass, *Ilm* ilmenite

ilmenite, K-feldspar, plagioclase and phlogopite. The observed reactions are suggestive of orthopyroxene and spinel replacement and formation of clinopyroxene + Ti-rich spinel, sometimes accompanied by ilmenite (Fig. 3H). Large spinel grains disintegrated by disequilibrium reactions are also found (Fig. 3I). The spinel relicts are rimmed by spinel-glass simplectites and surrounded by a typical veinlet assemblage of green clinopyroxene, glass, apatite and relics of orthopyroxene and olivine. Feldspars appear as irregular, patchy or prismatic crystals surrounded by glass, clinopyroxene, Ti-rich spinel and apatite.

Olivine Websterite (OWB) xenoliths

The OWB xenoliths are usually smaller than D/HZ/L xenoliths, rarely above 3–4 cm in diameter. They appear as rounded to subrounded nodules of dark-green to almost black colour. On the grounds of texture and mineral composition, the OWB samples can be divided into two sub-groups.

The first sub-group [termed spinel-rich olivine websterites (OWB_1)] consists of coarse-grained protogranular (Fig. 4A) samples Sb-3, X-20-5 and X-20-10, which contain significant amounts of chrome spinel (>2 vol%). They differ from D/HZ/L xenoliths in having low modal contents of olivine, which is present in the form of irregular concentrations or bands of fine-grained crystals. Orthopyroxene is coarse (sometimes $>4\times6$ mm), tabular and slightly undulose. Clinopyroxene is greenish and commonly situated in interstices between orthopyroxenes (opx). Spinel is large, sometimes >1 mm in diameter and euhedral (Fig. 4B). Plagioclase and rare K-feldspar are confined to reaction selvages around spinel grains. Along with clinopyroxene, glass and rare ilmenite, plagioclase and K-feldspar laths are perpendicular to partially resorbed spinel surfaces.

The second sub-group is termed spinel-poor olivine websterites (OWB_2) and consists of samples X-20-1, X-20-6, X-20-9 and X-20-11, all of which are much more altered than the OWB_1 xenoliths (Fig. 4C). They also differ from OWB_1 in their very scarce and small spinel grains. Orthopyroxene is predominant and forms tabular crystals, sometimes closely packed or surrounded by clinopyroxene and olivine. The olivine is often idiomorphic but it is difficult to observe due to alteration (Fig. 4D). Clinopyroxene is very small and usually distinguishable only in back-scatter electron images. Along with clinopyroxene and spinel, K-feldspar, plagioclase, apatite and rarely ilmenite are also present as interstitial minerals between orthopyroxene and altered olivine.

Cpx megacrysts (CPX-M)

These range from 5×3 cm to less than a few millimetre in length. They are very rarely accompanied by olivine, either as inclusions or attached grains. Contacts with the host groundmass are mostly sharp, but narrow (<100 μm) overgrowths of more iron-rich clinopyroxene are observed, indicating disequilibrium with the basanitic magma. Petrographically similar megacrysts are found in the Pannonian Basin and were described by Dobosi and Jenner (1999) and Dobosi et al. (2003) as well as in other localities worldwide (e.g. Aoki and Kushiro 1968; Binns et al. 1970; Wilshire and Shervais 1975; Irving and Frey 1984; Dal Negro et al. 1989; Righter and Carmichael 1993; Shaw and Eyzaguirre 2000; Brizi et al. 2003).

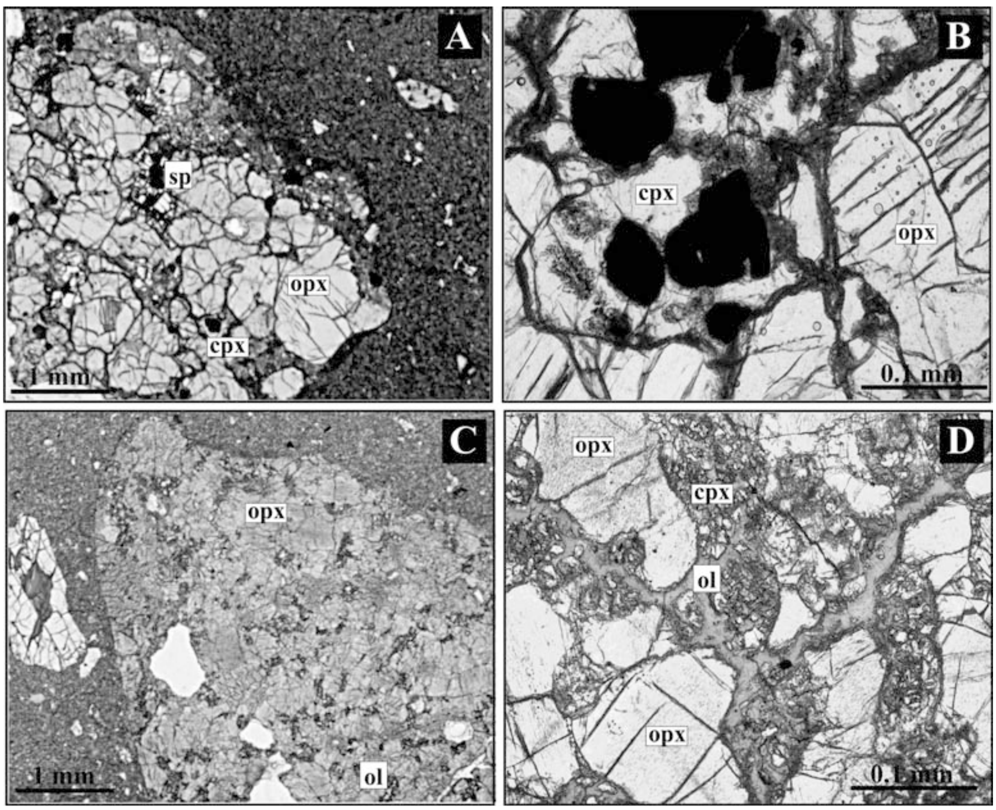

Fig. 4A–D **A** A PPL scanned image of a protogranular spinel-rich OWB_1 xenolith (X-20-5), **B** a PPL photomicrograph of coarse spinel grains concentrated within the OWB_1 xenolith; the spinels are enclosed by interstitial clinopyroxene and more euhedral and coarser orthopyroxene grains (sample X-20-5), **C** a PPL scanned image of a spinel-poor OWB_2 mantle xenolith (X-20-11), **D** a PPL photomicrograph of the same xenolith; intergranular spaces between tabular orthopyroxene crystals are filled by partly to intensively altered olivine relics sometimes with euhedral faces. For abbreviations see Fig. 3

Mineral chemistry

Mineral chemical analyses were performed at Birkbeck College, University of London using a Jeol 733 Superprobe. Data were collected at 15 kV, 20 nA beam current, for 100 s per analysis using an AN 10.000/55 s Link energy dispersive system with a ZAF4 correction program. Natural and synthetic minerals were used as standards. Analytical precision (2σ) evaluated by repeat analyses of individual crystals is 1–5% for oxides in concentrations in the range of > 20–2 wt% and < 10% for oxides in the range 0.5–2 wt%. Compositions of each phase were determined by averaging at least three points for the cores and at least two points for rims. Where present, exsolution lamellae in pyroxenes were avoided. Comparison is made with mantle xenoliths from the Pannonian Basin and French Massif Central, which were analysed on the same machine.

Olivine

Olivine is ubiquitous in all Serbian xenolith lithologies. Several olivine compositions can be recognized, corresponding to differences in lithology (Table 2). Olivines from D/HZ/L xenoliths are unzoned and generally show a rather uniform Mg# [$100 \times Mg/(Mg + Fe)$ mol%] between 89.5 and 91.8. Their NiO contents range from 0.5 to 0.7 wt%. These contents are very high compared to NiO concentrations in olivines from Poiana Rusca xenoliths reported by Downes et al. (1995), which do not exceed 0.40 wt%. Olivines from Cpx-L xenoliths tend to be less magnesian (Mg# between 86 and 88, except for X-20-2 with olivine of Mg# around 90) as are those in OWB xenoliths and olivine occurring with Cpx-M (Mg# mostly around 86). Olivines within pockets and veinlets in the D/HZ/L xenoliths show a wide scatter in composition, sometimes with very high Mg# of up to 92.9 but also as low as 78. The margins of olivine grains in contact with the basanite host are far more iron-rich and their Mg# values cluster around 75.

Figure 5 shows the "olivine-spinel mantle array" of Arai (1994). The D/HZ/L olivine-spinel compositions are typical of mantle peridotites worldwide, but those of the OWB_1 and OWB_2 samples are clearly different, particularly in the low Mg# of their olivines. Cpx-L also differ from the D/HZ/L samples. Two samples fall within the mantle array and one outside of it but all of them have lower Fo contents of olivine and lower Cr# in spinel compared to D/HZ/L xenoliths.

Orthopyroxene

Selected microprobe analyses of orthopyroxene are given in Table 3 and the compositional groups are illustrated in Fig. 6. Opx from the D/HZ/L samples show a uniform composition characterized by high MgO (Mg#

Table 2 Representative microprobe analyses of olivines from East Serbian mantle xenoliths

Xenolith type	D/HZ/L												Cpx-L			OWB_1			OWB_2			M	P and V				Reactions with host		
Sample no.	X-6	K-19	K-13	Sb-4	X-20-1a	X-20-3	X-20-7	stz-20-1	stz-20-3	stz-20-4	stz-20-4	stz-20-6	X-1	X-11/1	X-20-2	Sb-3	X-20-5	X-20-10	X-20-1	X-20-6	X-20-11a	X-10	X-11/2	X-20-3	X-20-7	stz-20-12	X-9s	X-20-1a	stz-20-7
SiO_2 (wt%)	42.02	42.38	41.05	41.27	41.05	41.26	41.36	41.11	41.32	41.32	41.15	41.18	41.77	41.29	41.37	40.68	40.08	40.67	39.99	39.83	39.87	40.16	42.12	40.76	40.29	39.13	40.34	39.42	38.38
FeO^t	7.63	7.58	9.33	8.14	8.80	8.71	8.53	8.76	8.03	8.73	8.46	9.41	11.01	12.13	9.68	12.93	12.50	12.11	13.27	15.31	12.88	12.67	6.84	10.44	12.59	19.97	17.59	16.67	21.31
MnO	0.16	0.00	0.15	0.06	0.06	0.13	0.14	0.05	0.14	0.11	0.18	0.06	0.15	0.15	0.09	0.08	0.17	0.10	0.19	0.30	0.27	0.09	0.12	0.11	0.47	0.27	0.42	0.28	0.35
MgO	48.84	48.94	49.18	50.64	49.11	49.51	49.77	49.53	49.77	49.54	49.16	48.86	46.55	45.37	49.02	46.17	45.97	46.85	45.30	43.99	45.19	43.59	49.62	47.57	45.66	39.90	40.49	42.84	38.50
CaO	0.03	0.01	0.04	0.05	0.03	0.10	0.05	0.08	0.08	0.07	0.15	0.06	0.19	0.15	0.15	0.11	0.10	0.09	0.15	0.16	0.16	0.23	0.03	0.27	0.43	0.30	0.31	0.12	0.34
NiO	0.63	0.63	0.68	0.47	0.54	0.58	0.53	0.64	0.57	0.58	0.39	0.55	0.58	0.63	0.60	0.49	0.56	0.49	0.55	0.34	0.62	0.47	0.49	0.49	0.72	0.26	0.51	0.75	0.48
Total	99.29	99.55	100.44	100.63	99.59	100.28	100.38	100.16	99.91	100.36	99.50	100.12	100.25	99.72	100.91	100.47	99.38	100.31	99.46	99.92	98.98	99.58	99.63	99.63	100.16	99.83	99.67	100.07	99.35
Mg#	91.95	90.68	90.38	91.73	90.86	90.53	91.23	90.98	91.70	91.00	91.19	90.22	88.28	86.96	90.03	86.66	86.76	87.33	85.88	83.66	86.22	85.98	92.82	89.92	86.61	78.08	80.23	82.09	76.30

FeO^t total Fe as FeO, Mg# = [$100 \times Mg/(Mg + Fe)$], *D/HZ/L* Dunite/harzburgite/lherzolite xenoliths, *Cpx-rich L* clinopyroxene-rich lherzolite, *OWB_1* spinel-rich olivine-websterites, *OWB_2* spinel-poor olivine-websterites, *M* megacrysts, *P and V* pockets and veins

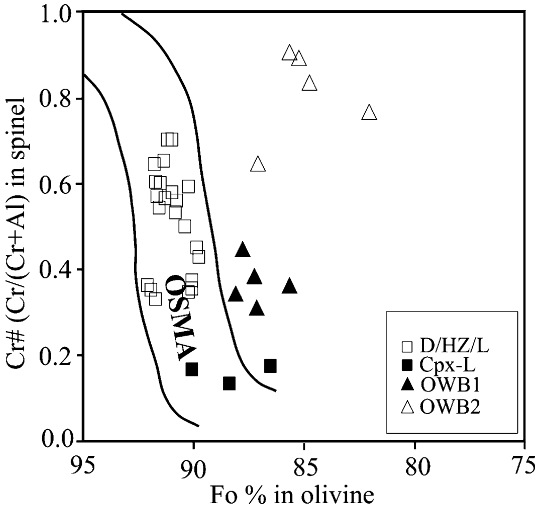

Fig. 5 Diagram of Fo percentage in olivine and Cr# =[Cr/(Cr + Al)] for co-existing spinels in mantle xenoliths of East Serbia. *D/HZ/L* dunite, harzburgite and lherzolite xenoliths, *Cpx-L* clinopyroxene rich lherzolite, *OWB_1* spinel-rich olivine websterite, *OWB_2* spinel-poor olivine websterite, *OSMA* olivine-spinel-mantle-array of Arai (1994)

=90–92), relatively low CaO (<0.80 wt%) and rather anomalously low Al_2O_3 contents (1.04–2.15, average 1.53 wt%). There is a broad negative correlation between Mg# and Al_2O_3. In comparison to orthopyroxene from Massif Central spinel peridotite xenoliths (Zangana 1995), which are regarded as normal mantle xenoliths or to orthopyroxene in Poiana Rusca xenoliths (Downes et al. 1995), the Serbian D/HZ/L orthopyroxenes are characterized by similar CaO (wt%) concentrations, slightly higher Mg# and Cr_2O_3 (wt%) and significantly lower alumina. Al_2O_3 contents range mostly around 3–4 wt% in opx from Poiana Rusca and Ray Pic xenoliths and 1–2 wt% in East Serbian mantle opx. Opx with <2 wt% Al_2O_3 are not common, although similar Al-poor opx are reported in xenoliths from the US (Smith and Riter 1997; Downes et al. 2004b, in press) and Japan (Morishita et al. 2003).

Orthopyroxenes from the Cpx-L xenoliths differ from those in the D/HZ/L xenoliths in having lower Mg# (<90) and higher CaO (>1 wt%) and Al_2O_3 (4–6 wt%). Opx from the spinel-rich OWB_1 xenoliths tend to have lower Mg# and higher Al_2O_3 than the D/HZ/L xenoliths, although they overlap to some extent with orthopyroxene from Cpx-L. However, orthopyroxene from spinel-poor OWB_2 samples have the lowest Mg# (<87) and also low CaO (~0.2 wt%) and Al_2O_3 (usually <2 wt%) concentrations.

Dunite/harzburgite/lherzolite samples appear to be well equilibrated judging from their regular variations of Mg# (opx) with Mg# (ol) (Fig. 7). They cluster close to the equilibrium line for protogranular mantle peridotite xenoliths from the Pannonian Basin reported by Embey-Isztin et al. (2001). Other olivine-orthopyroxene pairs in Serbian mantle xenoliths depart from the line.

Table 3 Representative microprobe analyses of orthopyroxene from East Serbian mantle xenoliths

Xenolith type	D/H/L															
Sample no.	X-6	K-19		K-13	Sb-4	X-20-7		X-20-15		stz-20-3		stz-20-4		stz-20-7	stz-20-9	stz-20-12
SiO_2	57.83	59.25	58.64	57.29	56.79	57.55	57.22	56.45	56.35	57.02	56.63	56.82	56.59	56.78	56.24	56.85
TiO_2	0.07	0.01	0.02	0.03	0.00	0.02	0.00	0.03	0.00	0.01	0.04	0.05	0.00	0.00	0.04	0.02
Al_2O_3	1.42	1.23	1.29	1.39	1.81	1.04	1.15	1.74	1.28	1.75	1.83	1.73	1.67	1.52	2.15	1.49
FeO	4.94	5.06	4.97	6.12	5.21	5.42	5.32	5.69	5.87	5.60	5.19	5.58	5.53	4.89	5.30	6.23
MnO	0.12	0.00	0.00	0.20	0.13	0.09	0.16	0.18	0.00	0.13	0.19	0.22	0.21	0.14	0.16	0.23
MgO	33.75	34.09	33.66	34.12	34.87	35.12	34.74	34.37	34.39	34.51	34.63	34.52	34.33	34.72	34.25	34.24
CaO	0.53	0.56	0.54	0.67	0.56	0.55	0.58	0.66	0.78	0.66	0.66	0.61	0.63	0.60	0.73	0.66
Na_2O_3	0.22	0.20	0.14	0.09	0.07	0.12	0.25	0.23	0.32	0.31	0.32	0.09	0.23	0.18	0.31	0.03
Cr_2O_3	0.40	0.40	0.50	0.48	0.47	0.38	0.47	0.44	0.84	0.48	0.47	0.50	0.42	0.55	0.51	0.42
Total	99.28	100.81	99.74	100.39	99.92	100.29	99.89	99.79	99.83	100.46	99.96	100.12	99.61	99.38	99.68	100.16
Mg#	92.24	92.31	92.36	90.58	92.08	91.91	91.86	91.26	91.26	91.49	91.99	91.38	91.42	92.48	91.80	90.43
Ca#	1.11	1.18	1.13	1.38	1.14	1.12	1.19	1.36	1.60	1.35	1.35	1.25	1.31	1.22	1.50	1.36
Al p.f.u.	0.0576	0.0493	0.0519	0.0562	0.0729	0.0419	0.0465	0.0705	0.0519	0.0703	0.0740	0.0697	0.0675	0.0616	0.0871	0.0602

Xenolith type	Cpx-L				OWB_1						OWB_2				
Sample no.	X-1	X-11/1		X-20-2	Sb-3	X-20-5		X-20-10			X-20-1		X-20-6	X-20-9a	X-20-11a
SiO_2	55.95	55.86	55.66	53.60	55.41	56.11	55.55	55.02	55.46	57.34	55.52	55.35	50.81	56.75	55.44
TiO_2	0.19	0.17	0.19	0.23	0.06	0.04	0.05	0.25	0.08	0.11	0.09	0.11	0.17	0.17	0.06
Al_2O_3	4.45	4.11	4.57	6.24	3.22	2.38	3.27	2.84	3.68	0.23	1.82	2.10	1.14	2.02	1.75
FeO	6.86	7.75	7.27	6.11	6.82	6.48	6.68	6.97	7.23	7.80	9.74	9.95	11.64	8.82	8.86
MnO	0.19	0.11	0.22	0.23	0.13	0.15	0.11	0.06	0.38	0.14	0.18	0.17	0.10	0.05	0.16
MgO	30.73	30.49	30.12	31.39	32.38	33.48	32.54	32.97	31.98	32.58	31.25	31.64	36.06	32.70	32.14
CaO	1.04	0.89	1.11	1.64	0.85	0.44	0.80	0.64	0.98	1.81	0.19	0.22	0.22	0.21	0.15
Na_2O_3	0.26	0.25	0.24	0.21	0.19	0.14	0.18	0.12	0.20	0.30	0.22	0.15	0.11	0.20	0.13
Cr_2O_3	0.49	0.50	0.46	0.75	0.63	0.64	0.84	0.77	0.62	0.47	0.26	0.39	0.26	0.35	0.27
Total	100.17	100.13	99.85	100.40	99.69	99.86	100.02	99.65	100.61	100.99	99.27	100.08	100.51	101.27	98.97
Mg#	88.59	87.35	87.75	89.83	89.25	89.99	89.50	89.33	88.21	87.98	84.88	84.78	84.51	86.79	86.39
Ca#	2.37	2.06	2.59	3.62	1.85	0.94	1.75	1.38	2.16	3.84	0.43	0.50	0.44	0.46	0.33
Al p.f.u.	0.1817	0.1681	0.1871	0.2526	0.1312	0.0966	0.1331	0.1153	0.1493	0.0095	0.0754	0.0862	0.0467	0.0818	0.0723

Ca# = [100 × Ca/(Ca + Mg)], abbreviations as in Table 1

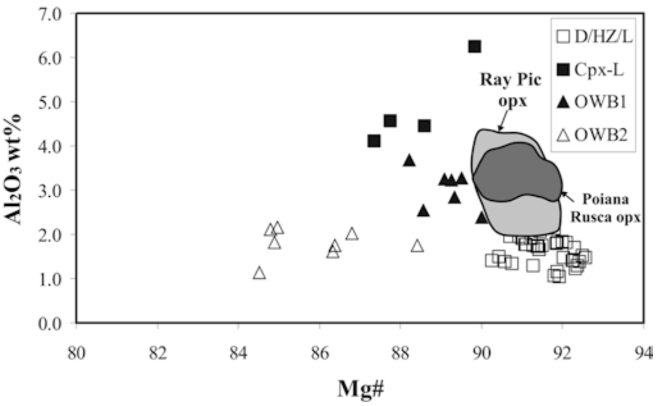

Fig. 6 Mg# = [100 × Mg/(Mg + Fe)] vs. Al_2O_3 (wt%) diagram for orthopyroxenes from mantle xenoliths of East Serbia; the composition of orthopyroxenes from Poiana Rusca (Downes et al. 1995) and Ray Pic (Zangana 1995) spinel peridotite xenoliths is also shown; abbreviations as in Fig. 5

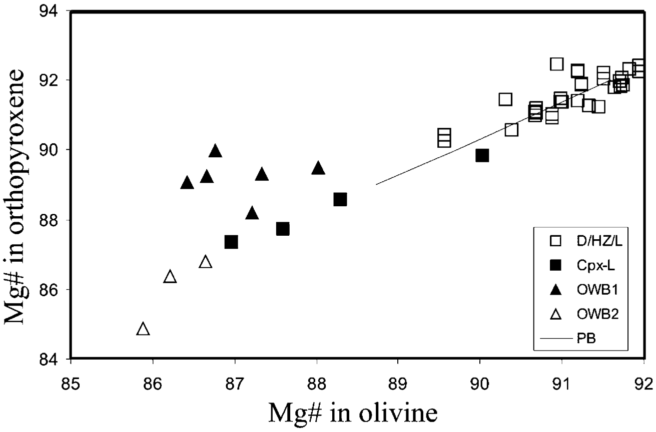

Fig. 7 Mg# = [100 × Mg/(Mg + Fe)] in olivine vs. Mg# = [100 × Mg/(Mg + Fe)] in orthopyroxene for mantle xenoliths of East Serbia; the equilibrium line (*PB*) shows the compositions of olivine-orthopyroxene pairs for mantle xenoliths from the Pannonian Basin (Embey-Isztin et al. 2001); abbreviations as in Fig. 5

Clinopyroxene

All cpx from D/HZ/L and OWB xenoliths are diopside or endiopside. In contrast, megacryst cpx and those formed by reactions with the basanitic host are richer in Fe and Ca, and tend towards Ca-rich salite. However, cpx is more heterogeneous in composition than olivine and orthopyroxene. Selected microprobe analyses are shown in Table 4 and compositional groups are presented in Fig. 8.

Dunite/harzburgite/lherzolite cpx are much more common as small constituents of patchy pockets and veinlets but rarely occur as coarser grains or interstitial irregular crystals. Both types of cpx are characterized by rather low Na_2O contents (< 1 wt%) (Fig. 8A) in comparison to cpx from Poiana Rusca (mostly > 1 wt% Na_2O; Downes et al. 1995). They also have the highest Mg#s (> 88) and very variable TiO_2 (0.1–3.2 wt%). With

Table 4 Representative microprobe analyses of clinopyroxene from East Serbian mantle xenoliths

Xenolith type	D/HZ/L						Cpx-L					OWB_1				OWB_2			M					P and V				
Sample no.	X-6	K-13	X-20-7	X-20-15	stz-20-3	stz-20-12	X-1		X-11/1	X-20-2		Sb-3	X-20-5	X-20-10		X-20-1	X-20-6	X-20-9	X-10		K-8	X-9s		X-11/2		Sb-4	X-20-7	X-20-15
SiO_2	55.53	52.96	54.57	53.68	54.28	53.08	50.86	51.07	53.15	50.31	49.92	52.03	52.23	52.83	52.32	52.78	53.08	53.89	50.56	50.12	47.56	49.14	48.31	52.61	48.90	48.64	49.83	48.12
TiO_2	0.40	0.49	0.05	0.07	0.14	0.26	0.86	1.15	0.57	0.74	0.84	0.57	0.31	0.18	0.37	0.93	0.37	0.40	0.93	0.99	1.42	0.71	0.91	0.86	3.24	0.29	0.28	1.02
Al_2O_3	0.61	2.20	1.41	1.87	0.32	2.35	5.85	6.83	5.43	7.28	6.43	5.48	5.77	5.81	5.85	1.21	2.49	1.36	6.86	7.59	10.11	7.85	8.73	3.65	5.98	7.01	6.51	8.04
FeO^t	3.19	3.34	2.53	2.47	3.07	2.89	3.69	3.97	4.09	3.79	3.44	3.60	3.56	3.78	4.03	4.30	3.52	4.83	4.50	4.58	4.92	2.87	2.97	2.90	3.31	2.38	2.62	3.63
MnO	0.15	0.22	0.15	0.11	0.19	0.24	0.08	0.14	0.09	0.12	0.21	0.32	0.20	0.20	0.17	0.55	0.17	0.12	0.07	0.12	0.12	0.03	0.07	0.08	0.07	0.29	0.34	0.19
MgO	19.17	17.15	17.63	17.44	19.02	16.60	15.04	14.51	16.27	17.24	15.61	15.82	15.39	15.62	15.86	17.46	18.23	17.84	14.62	14.74	13.86	14.31	13.77	16.27	15.50	14.82	15.93	14.75
CaO	19.33	22.37	23.34	22.99	19.75	21.67	21.47	20.66	19.88	17.61	22.08	19.34	18.54	18.65	18.66	19.80	20.74	20.09	20.69	20.01	20.43	21.44	21.70	22.05	21.01	21.98	20.28	20.06
Na_2O	0.78	0.48	0.56	0.54	0.70	0.80	0.93	0.97	1.00	0.85	0.60	1.22	1.34	1.30	1.26	1.16	0.55	0.67	0.88	0.92	0.74	0.91	0.87	0.81	0.90	0.62	0.77	0.77
Cr_2O_3	0.95	0.59	0.46	0.71	1.51	1.52	1.01	1.11	0.72	1.17	1.30	1.59	1.81	1.78	1.68	1.96	1.01	1.33	0.55	0.56	0.35	3.27	3.23	1.68	1.33	3.42	3.99	2.63
Total	100.13	99.80	100.69	99.90	98.98	99.39	99.79	100.42	101.20	99.11	100.43	99.98	99.14	100.15	100.21	100.14	100.15	100.54	99.66	99.62	99.50	100.53	100.56	100.91	100.24	99.45	100.55	99.21
Mg#	91.09	89.51	92.15	92.33	91.26	90.45	87.68	86.27	87.40	88.73	88.37	87.77	87.95	87.49	87.08	86.57	89.81	86.53	85.07	84.84	83.04	89.78	88.99	90.51	88.35	90.77	90.52	87.30
Ca#	42.01	48.41	48.75	48.64	42.74	48.41	50.62	50.51	46.76	42.34	50.43	47.14	46.40	46.18	45.82	44.77	44.98	44.74	50.39	49.39	51.45	51.85	53.10	49.44	49.86	51.64	47.86	49.42
Cr#	51.02	14.97	17.76	19.92	75.61	30.27	10.46	10.06	8.21	9.76	12.09	16.79	17.36	17.08	16.17	48.99	22.17	39.79	5.13	4.74	2.25	21.81	19.90	31.27	20.99	24.89	29.31	17.84
Al p.f.u.	0.0259	0.0944	0.0599	0.0800	0.0139	0.1012	0.2522	0.2932	0.2290	0.3124	0.2747	0.2341	0.2480	0.2474	0.2495	0.0519	0.1060	0.0579	0.2958	0.3273	0.4371	0.3367	0.3746	0.1556	0.2586	0.3038	0.2787	0.3490

Cr# = [100 × Cr/(Cr + Al)], *P and V* pockets and veins, *M* megacrysts, other abbreviations as in Table 1

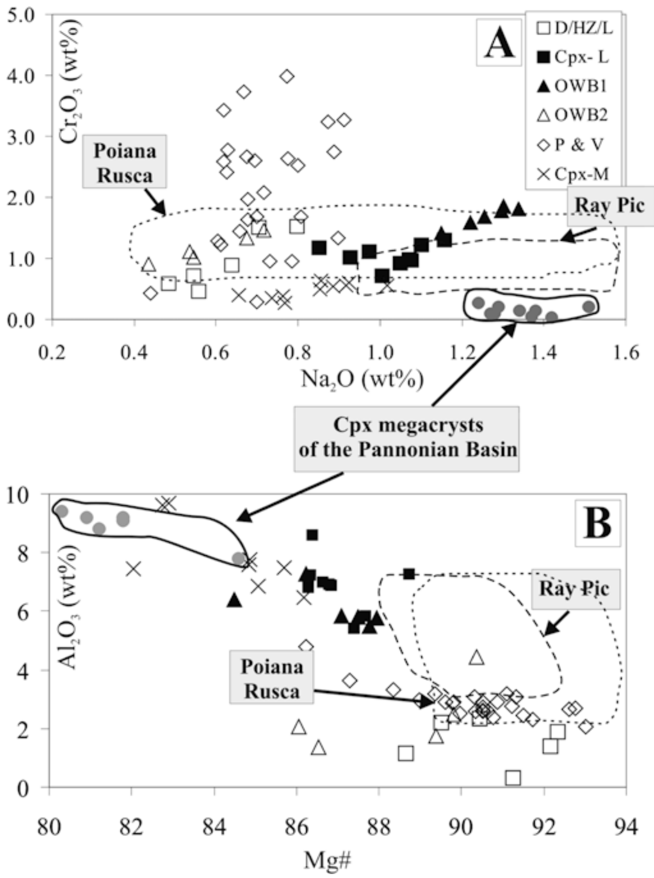

Fig. 8A,B **A** Na_2O vs. Cr_2O_3 (wt%) and **B** Mg# = [100 × Mg/(Mg + Fe)] vs. Al_2O_3 (wt%) for clinopyroxenes from various mantle xenoliths of East Serbia; the composition of clinopyroxene from xenoliths of Poiana Rusca (Downes et al. 1995) and Ray Pic (Zangana 1995) and of clinopyroxene megacrysts from the Pannonian Basin (Dobosi et al. 2003) is also shown. *P* and *V* clinopyroxenes from pockets and veins, *Cpx-M* clinopyroxene megacrysts, other abbreviations as in Fig. 5

respect to clinopyroxenes in Ray Pic mantle xenoliths (Zangana 1995), they are Cr_2O_3-rich and Na_2O-poor, suggestive of rather refractory mantle composition beneath East Serbia. However, coarser cpx from the D/HZ/L xenoliths differ from cpx from pockets and veinlets in the same xenoliths in that the latter have substantially higher Al and Cr and significantly lower SiO_2 contents. Al_2O_3 and Cr_2O_3 contents range 4–9 and 1.5–4 wt%, respectively in clinopyroxene from metasomatic pockets and up to 2.3 wt% and mostly < 1.5 wt%, respectively in coarser clinopyroxene. SiO_2 contents are mostly ~49 wt% in clinopyroxene from pockets and ~54 wt% in coarser clinopyroxene from D/HZ/L.

Clinopyroxenes from Cpx-L and OWB_1 samples are characterized by lower Mg# (< 87). Their TiO_2 and Al_2O_3 contents are higher than in coarser cpx from D/HZ/L xenoliths and are much more akin to pocket cpx (around 0.8 wt% TiO_2 and > 5 wt% Al_2O_3). The highest Na_2O contents (always > 1 wt%) are found in cpx from OWB_1 xenoliths. Cpx-M reach Mg#s as low as 82 and Al_2O_3 up to 10 wt% (Fig. 8B) and show the lowest Cr contents (< 1 wt% Cr_2O_3). They are similar in composition to Cpx-M from the western Pannonian Basin (Dobosi and Jenner 1999; Dobosi et al. 2003). Besides similar Mg#s and alumina contents they all show rather high Al partition to the octahedral site. Al^{VI}/Al^{IV} ratios in Cpx-M from the Pannonian Basin range from 0.7 to 1.05 which is similar to East Serbian Cpx-M (0.4–1), cpx from Cpx-L (0.4–1.3), and cpx from OWB_1 (0.4–1.7). However, comparing the megacrysts from the Pannonian Basin to those in East Serbia, it is apparent that the former differ in their much higher Na_2O contents (around 1.3 wt%) and very low Cr_2O_3 concentrations (usually below detection limit). In addition, cpx from Cpx-L, OWB_1 and megacrysts show similar Al and Ti contents to cpx from the vein pyroxenites and composite peridotite xenoliths of Eifel (Witt-Eickschen and Kramm 1998).

Clinopyroxenes from the OWB_2 group have very variable Mg#s (85–90) differing from those in Cpx-L and OWB_1 samples in having lower Na_2O (< 0.70 wt%) and Al_2O_3 (1–2.5 wt%) (Fig. 8A, B) and especially in their very low Al^{VI}/Al^{IV} ratios (usually < 0.2).

Clinopyroxenes formed in reactions with the host basanite magma have the lowest MgO# (approaching 70), very low Cr_2O_3 (around 0.25 wt%) and extremely high Ti and Al (up to 3 wt% TiO_2 and 8 wt% Al_2O_3).

Spinel

Spinel is extremely variable in composition (Table 5). Those in D/HZ/L xenoliths have Cr# ranging from 43 to 61 and low TiO_2 contents (< 0.2 wt%). Those from pockets and veins have similar Cr# (35–50) and higher and variable TiO_2 contents (up to 9 wt%, mostly around 2 wt%) in comparison to D/HZ/L spinels. Spinels from Cpx-L show the lowest Cr# of all the East Serbian xenolith suites (Cr# < 20). They have rather uniform TiO_2 contents (~0.5 wt%). Similar to them are spinels from OWB_1 xenoliths (Cr# ~30, TiO_2~1 wt%). Spinels occurring in OWB_2 xenoliths are mostly Cr-rich (Cr# = 75–95) and have very high TiO_2 contents (3–10 wt%).

On the olivine-spinel diagram (Fig. 5), the D/HZ/L and some of the Cpx-L phases follow the "mantle array" of Arai (1994) with increasing Cr# in spinel as Fo content of the olivine increases, but those from the OWB xenoliths fall away from this worldwide trend. The OWB xenoliths separate clearly into two groups with different spinel compositions, the OWB_1 xenoliths having lower Cr# in their spinels than the OWB_2 xenoliths, which are extremely Cr-rich.

Figure 9 shows that the major D/HZ/L spinel population form a correlation between Cr# and Fe# as usually seen in spinels from mantle xenoliths worldwide (Barnes and Roeder 2001). It is suggestive of the Al–Cr trend generally explained by spinel equilibration with mantle silicates (Irvine 1967; Dick and Bullen 1984; Barnes and Roeder 2001). The Al–Cr substitution is overprinted by a Fe–Ti trend (e.g. Roeder and Campbell

Table 5 Representative electron microprobe analyses of spinel from East Serbian mantle xenoliths

Xenolith type	D/H/L										Cpx-L					OWB_1				OWB_2						P and V				
Sample no.	X-6		X-11/2	K-13	Sb-4	X-20-3	X-20-1a	X-20-15	stz-20-3	stz-20-9	X-1	X-11/1			X-20-2	Sb-3		X-20-5	X-20-10	X-20-1	X-20-6		X-20-9a		X-20-11a	X-6	X-9s	X-11/2		K-19
SiO_2	0.25	0.29	0.32	0.30	0.27	0.19	0.31	0.24	0.23	0.26	0.31	0.32	0.34	0.25	0.21	0.19	0.26	0.20	0.21	0.42	0.40	1.16	0.36	0.35	0.68	0.40	0.36	0.72	0.57	0.32
TiO_2	0.21	0.22	0.17	0.35	0.10	0.33	0.06	0.17	0.30	0.15	0.51	0.38	0.55	0.54	0.51	1.36	1.16	0.84	1.19	3.52	10.47	3.23	6.49	3.01	5.63	1.78	9.94	2.59	2.83	0.24
Al_2O_3	20.20	20.58	20.62	19.57	22.52	29.96	22.94	21.65	21.72	20.79	53.27	49.69	48.90	50.29	50.74	35.60	39.12	35.48	34.23	1.51	1.97	0.89	4.41	10.49	2.78	26.10	19.13	19.07	30.87	37.34
FeO^t	17.87	18.13	17.32	21.59	18.53	16.43	21.77	20.08	20.36	20.66	12.74	14.02	14.28	14.20	12.02	20.07	19.35	19.06	19.08	33.73	43.68	34.50	38.12	31.52	37.76	18.47	43.33	23.48	22.22	11.74
MnO	0.30	0.14	0.06	3.26	3.32	2.75	3.16	3.53	3.57	3.40	0.02	0.20	0.18	0.11	1.25	2.04	1.71	2.35	2.29	4.33	3.06	4.59	3.55	3.96	3.79	0.22	0.33	0.25	0.24	
MgO	12.97	13.01	13.26	12.99	14.17	16.02	13.46	13.77	13.82	14.20	19.09	18.08	18.12	18.19	20.16	15.89	16.64	15.46	15.88	5.81	5.13	4.75	6.61	6.75	5.39	14.19	7.65	12.47	13.40	17.76
CaO	0.04	0.07	0.02	0.02	0.06	0.03	0.01	0.04	0.01	0.05	0.03	0.03	0.04	0.03	0.02	0.04	0.03	0.03	0.04	0.11	0.25	0.11	0.27	0.32	0.26	0.15	0.16	0.08	0.24	0.43
Cr_2O_3	47.97	47.71	46.54	42.43	41.41	34.66	38.21	41.48	41.05	40.76	13.36	16.68	16.98	16.37	15.01	25.35	21.91	27.68	27.47	50.18	33.33	51.34	40.23	43.50	43.95	36.91	14.24	41.19	29.89	32.12
Total	99.81	100.17	98.31	100.51	100.39	100.36	99.91	100.97	101.06	100.26	99.33	99.41	99.39	99.98	99.92	100.54	100.19	101.10	100.37	99.60	98.29	100.57	100.04	99.89	100.24	98.23	95.15	99.87	100.26	99.95
Cr#	61.44	60.86	60.22	59.24	55.23	43.69	52.82	56.25	56.41	56.81	14.40	18.38	18.89	17.93	16.56	32.38	27.34	34.36	35.03	95.62	86.79	97.50	85.81	74.75	91.40	48.79	42.47	58.48	40.71	36.58
Fe#	40.24	40.59	38.84	35.98	30.77	26.38	34.27	32.36	33.22	30.04	25.86	28.09	28.03	28.39	19.51	31.55	29.80	32.18	30.48	68.78	76.19	74.80	68.11	64.83	73.22	42.20	74.43	50.10	47.85	27.05

Fe# = [100 × Fe/(Fe + Mg)], abbreviations as in Table 1

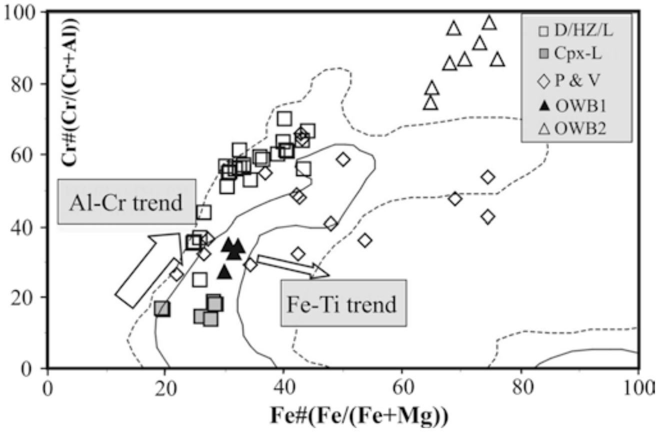

Fig. 9 Fe# = [100 × Fe/(Fe + Mg)] vs. Cr# = [100 × Cr/(Cr + Al)] for spinels in East Serbian mantle xenoliths; fields of spinel compositions (data base of 26,000 spinel analyses) from worldwide mantle xenoliths are also shown; data density plots are defined by 50th (*dashed line*) and 90th (*full line*) percentile contours (Barnes and Roeder 2001)

1985) shown by some spinel grains from pockets and veinlets (Fig. 9). This spinel shows an increase in Fe# accompanied by decreasing of Cr# and increasing of TiO_2 (sometimes > 10 wt%). Spinels adjacent to the host basanite have low totals, suggesting increased Fe^{3+} contents, and are very rich in TiO_2 (~20 wt%), approaching the composition of titanomagnetites from the basanitic groundmass (Jovanović et al. 2001).

The OWB_1 xenoliths have Al- and Ti-rich spinels (Figs. 9 and 10B). In contrast, the rare tiny spinels within the OWB_2 xenoliths are much richer in Cr, with Cr#s up to 98, and they have variable and sometimes very high TiO_2 contents (~10 wt%). In the Al_2O_3 (wt%) vs. TiO_2 (wt%) diagram (Fig. 10A), the vast majority of the D/HZ/L spinels plot within the supra-subduction zone (SSZ) field or inside the overlap between the SSZ and MORB fields of Kamenetsky et al. (2001). Spinels from OWB_1 and Cpx-L samples form separate groups outside the field of spinel from SSZ peridotites and towards more fertile compositions. In contrast, spinel from OWB_2 xenoliths plot within or close to the uppermost corner of the field of spinels crystallized from magma, as is also apparent from the Cr_2O_3 (wt%) vs. Al_2O_3 (wt%) diagram (Fig. 10B). They entirely plot within the field of "arc cumulate spinels" (Conrad and Kay 1984) and outside of the mantle array (Kepezhinskas et al. 1995), which hosts all other spinel groups. Compositions of spinels in veinlets and pockets show a large scatter. Some of them plot within the field of SSZ peridotite spinels but many are displaced to higher TiO_2 contents.

Other phases from metasomatic pockets and veinlets

The cpx-rich pockets discussed above also contain various amounts of altered glass, feldspar, ilmenite, apatite and very rare phlogopite. Microprobe analyses of minerals from pockets and veinlets are presented in Table 6.

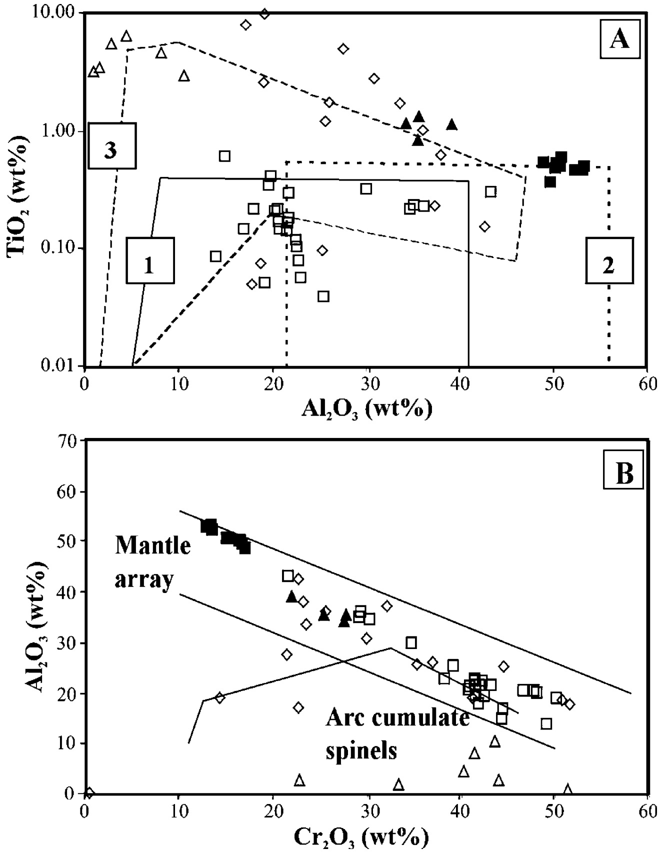

Fig. 10A,B **A** Al_2O_3 vs. TiO_2 (wt%) and **B** Cr_2O_3 vs. Al_2O_3 (wt%) for spinels occurring in East Serbian mantle xenoliths; fields in (**A**) are for spinels from supra-subduction zone (*SSZ*) peridotites (*1*), MORB peridotites (*2*) and magmatic spinels (*3*) (Kamenetsky et al. 2001), mantle array and field for arc cumulate spinels in (**B**) are from Conrad and Kay (1984) and Kepezhinskas et al. (1995), respectively; symbols as in Fig. 9

Feldspar is rare in mantle xenoliths (e.g. Ionov et al. 1995a, b, 1999; Gregoire et al. 1997). In the Serbian D/HZ/L xenoliths, it is mainly calcic plagioclase (An_{50-70}, $Or_{2-6.5}$). It is richer in Na and K than plagioclase from the basanitic groundmass ($An_{>75}$, $Or_{0-4.5}$, Jovanović et al. 2001). In the OWB samples, plagioclase is even more albitic and orthoclase-rich (An_{39-66}, up to Or_{11}) and is commonly accompanied by K-feldspar (Or_{59-66}). Ilmenite is found only in a few D/HZ/L and OWB xenoliths. It has a uniform composition characterized by TiO_2 contents ranging from 51 to 54 wt% and Fe# > 70. Phlogopite has been found in only one harzburgite xenolith. It shows relatively high Mg# (> 0.80) coupled with very high TiO_2 (> 10 wt%) and moderate Al_2O_3 (15 wt%) and Cr_2O_3 (ca. 1 wt%). The glass was too altered to be analysed by EMP.

Temperature, pressure and fO_2 estimates

Average values of temperature and oxygen fugacity calculated according to different authors are given in Table 7.

Calculated temperatures for D/HZ/L xenoliths mostly range between 950 and 1,100°C. The most uniform values were obtained using the geothermometer of Mercier (1980) based on orthopyroxene composition (994–1,046°C). Also uniform but somewhat lower temperature values gave Brey and Kohler (1990) based on Ca contents in orthopyroxene (918–988°C). Temperatures in excess of 1,100°C were calculated only using two-pyroxene thermometers of Wood and Banno (1973) and Wells (1977). Average calculated temperatures for Cpx-L and OWB_1 xenoliths range from 970–1,195°C and they are uniform regardless of the geothermometers used (Table 7). The thermometric calculations based on mineral composition of OWB_2 xenoliths show clear differences between the two-pyroxene thermometers and those using only orthopyroxene composition. The thermometers of Wood and Banno (1973), Wells (1977), Brey and Kohler (1990) (BKN) and Mercier (1980) (di/sp) reveal a range between 1,009 and 1,182°C whereas the thermometers of Mercier (1980) and Brey and Kohler (1990) show essentially lower temperature values ranging 827–866°C and 731 and 797°C, respectively.

Pressure cannot be calculated on the basis of mineral composition but only regarding the presence of spinel instead of garnet as the aluminous phase. Accordingly the deepest regions sampled by Serbian basanites correspond to depths up to 70 km or pressures around 2 GPa.

Oxygen fugacites were calculated using the methods of Ballhaus et al. (1991) and Wood (1991). Average estimates based on coarse spinels from the D/HZ/L xenoliths yield a large variation from –0.5 to + 1.8 log(fO_2) units relative to the FMQ buffer (ΔFMQ) and display little differences between the two methods. Cpx-L and OWB_1 xenoliths indicate conditions close to the FMQ buffer with values ranging between –0.5 and 0 log(fO_2) units. All estimates of OWB_2 xenoliths show substantially more oxidizing conditions revealing + 1–+ 2.4 log(fO_2) units relative to the FMQ buffer. However, they show larger differences between the methods in that the method Ballhaus et al. (1991) gave higher values for 0.4–1 log(fO_2) units than the method of Wood (1991).

Trace elements in clinopyroxene

In situ LA-ICP-MS analyses of clinopyroxene have been carried out using a VG Plasma QuadPQII machine at the Institute of Geography and Earth Sciences, University of Wales in Aberystwyth. Calibration was made against a synthetic glass reference material (NIST 610), and an estimated standard deviation < 15% relative, at parts per million level was obtained. Mean Si concentrations (obtained by microprobe) in ablated cpx was used for internal standardization during the quantification of LA-ICP-MS data. We analysed the natural clinopyroxene RP91-17 and obtained data for REE

Table 6 Representative microprobe analyses of plagioclase feldspars (Pl), potash-feldspars (K-f), ilmenite (Ilm) and phlogopite (Phl) from East Serbian mantle xenoliths

Type	D/HZ/L				OWB_1				OWB_2				
Sample no.	Sb-4		STZ-20-1		X-20-5		X-20-10		X-20-1			X-20-11	
Mineral	pl	pl	pl	pl	pl	pl	pl	kf	kf	kf	kf	kf	kf
SiO_2	56.71	56.87	55.62	55.38	55.98	54.61	56.92	66.37	64.55	65.73	65.67	65.09	65.48
Al_2O_3	28.08	28.59	28.36	29.85	29.76	29.87	28.18	20.12	21.68	22.11	21.11	20.93	21.00
CaO	9.63	9.65	9.80	9.65	9.73	11.18	10.13	0.69	0.00	0.00	0.08	0.25	0.32
Na_2O	3.98	3.55	3.28	3.21	3.28	2.97	3.43	3.13	3.32	3.18	3.38	3.76	3.33
K_2O	0.55	0.39	0.87	0.74	0.39	0.27	0.48	9.32	9.72	8.50	8.87	8.87	8.86
BaO	0.65	0.50	0.54	0.55	0.60	0.44	0.54	0.66	0.06	0.00	0.36	0.46	0.39
Total	99.60	99.55	98.47	99.39	99.74	99.34	99.69	100.28	99.33	99.52	99.47	99.36	99.38
Or	5.29	4.64	6.54	3.31	4.19	2.83	4.52	64.10	65.77	63.23	64.19	61.30	59.51
Ab	43.03	33.15	37.38	37.21	36.32	31.54	36.29	31.98	34.23	36.78	35.32	37.05	38.43
An	51.68	62.20	56.08	59.48	59.49	65.64	59.19	3.92	0.00	0.00	0.08	1.65	2.06

Type	D/HZ/L	Cpx-L		OWB_1	OWB_2		Type	D/HZ/L			
Sample no.	stz-20-1	X-11/1		X-20-10	X-20-9	X-20-11	Sample no.	stz-20-1			
Mineral	ilm	ilm	ilm	ilm	ilm	ilm	Mineral	phl	phl	phl	phl
SiO_2	0.33	0.40	0.35	0.37	0.45	0.28	SiO_2	35.11	37.23	29.98	34.18
TiO_2	53.15	53.32	53.87	51.11	52.87	51.31	TiO_2	11.95	11.61	14.64	8.13
Al_2O_3	0.20	0.29	0.23	0.07	0.17	0.05	Al_2O_3	15.80	14.24	12.29	17.45
FeO	34.07	35.58	34.82	35.33	33.80	34.02	FeO	5.96	6.22	15.26	22.81
MnO	0.59	0.43	0.55	0.79	0.44	0.45	MnO	0.18	0.00	0.38	0.70
MgO	7.85	6.53	6.97	6.65	7.95	7.61	MgO	16.18	16.88	13.40	2.55
CaO	0.07	0.07	0.10	0.16	0.12	1.15	CaO	0.18	0.15	0.00	0.27
Cr_2O_3	1.30	0.46	0.44	1.62	2.16	2.21	Na_2O	0.76	0.83	0.92	3.02
Total	97.56	97.10	97.34	96.10	97.96	97.07	K_2O	8.52	8.79	6.90	1.41
Cr#	81.35	51.50	55.68	93.81	89.75	96.92	Cr_2O_3	0.53	0.67	3.98	7.54
Mg#	29.11	24.65	26.30	25.12	29.54	28.50	Total	95.16	96.62	97.76	98.06
Fe#	70.89	75.35	73.70	74.88	70.46	71.50	Mg#	0.83	0.83	0.61	0.17

Abbreviations as in Table 1

within less than 15% relative of the values quoted by Mason et al. (1999). Trace element concentrations were averaged from three measurements. A rastering mode of ablation was used in all cases except for sample Sb-4 (pocket cpx) where laser pits of around 30 μm in diameter were made.

Coarse interstitial clinopyroxene crystals from a D/HZ/L xenolith (X-6), tiny cpx from pockets (SB-4), coarse cpx from two Cpx-L samples (X-1 and X-11-1), clinopyroxene from one OWB_1 sample (Sb-3) and a Cpx-M (K-8) have been analysed. Unfortunately, cpx from OWB_2 were too small to be ablated. Some variability of the analyses for cpx from the pockets may be due to difficulties arising from the ablation of small (usually <30 μm) pyroxene crystals. Trace element composition of cpx from these six xenoliths are shown in Table 8. Figure 11 shows the chondrite-normalized (Sun and McDonough 1989) trace element abundances of the studied cpx. For comparison, normalized trace element contents of clinopyroxenes in xenoliths from Massif Central (Mason et al. 1999), Eifel (Witt-Eickschen and Kramm 1998) and Cpx-M from the Pannonian Basin (Dobosi and Jenner 1999; Dobosi et al. 2003) are also presented.

Coarse-grained cpx from the D/HZ/L xenolith (X-6) display patterns characterized by a moderately steep REE-fractionation (La_N/Lu_N = 8–9) and only a slight depletion in HFSE and Sr (Fig. 11A). On the same diagram two cpx from the French Massif Central (Mason et al. 1999; Zangana et al. 1999) are also shown. Clinopyroxene from a LREE-enriched harzburgite from the Massif Central (RP 83-72) shows certain similarities to the clinopyroxene from the East Serbian D/HZ/L sample X-6. Their LREE contents and ratios are very similar while major differences are in HREE and HFSE contents which are higher in the Serbian D/HZ/L clinopyroxene. Both cpx show similar Zr_N/Hf_N fractionation of around 0.8. Massif Central pyroxenite xenolith BT-36 shows overall a similar pattern to Serbian D/HZ/L clinopyroxene, displaying a similar La_N/Lu_N of 10, but has a much more pronounced Sr negative spike and lacks Zr–Hf depletion.

Clinopyroxenes from pockets and veinlets (sample SB-4) show a greater degree of HREE depletion and a distinctive positive Sr anomaly (Fig. 11B). However, some samples show a zigzagging pattern, which may be due to ablation of some adjacent material other than clinopyroxene. These cpx show similar or slightly lower

Table 7 Average calculated values of temperature and oxygen fugacity for East Serbian mantle xenoliths

Xenolith	Sample	Temperature (°C)						fO_2 (ΔFMQ)	
		Wood and Banno (1973)	Wells (1977)	Brey and Kohler (1990) (BKN)	Brey and Kohler (1990) (Ca-op)	Mercier (1980) (di/sp)	Mercier (1980) (en/sp)	Ballhaus et al (1991)	Wood (1991)
D/HZ/L	X-6	1,133	1,151	1,184	927	977	994	−0.394	−0.210
	X-11/2	1,086	989	976	920	998	1,003	−0.525	−0.497
	K-19	963	934	775	925	954	1,004		
	K-13	1,047	942	940	956	1,021	1,028	1.396	1.317
	Sb-4				918		998	1.339	1.352
	X-20-1a								1.657
	X-20-3								0.877
	X-20-7	1,006	978	829	925	959	1,024	1.856	1.639
	Stz-20-1	1,130	1,119	1,162	946	979	1,018		
	Stz-20-3				953		1,028	1.632	1.550
	Stz-20-2	1,005	974	988	986	989	1,045		
	Stz-20-4			944			1,018	1.158	1.097
	Stz-20-6							0.928	
	Stz-20-7	1,030	1,014	1,033	988	1,023	1,017	1.801	1.223
	Stz-20-9				977		1,046	1.285	0.654
Cpx-L	X-1	1,110	1,038	1,070	1,063	1,023	1,123	−2.483	−2.431
	X-11/1	1,126	1,071	1,104	1,024	1,132	1,089	−0.576	−0.559
	X-20-2	1,071	997	970	1,195	993	1,120	−0.145	0.040
OWB_1	Sb-3	1,121	1,042	1,116	1,014	1,126	1,076	0.593	−0.128
	X-20-5	1,133	1,053	1,149	1,011	1,135	1,070	0.335	−0.411
	X-20-10	1,145	1,079	1,153	1,048	1,146	1,103	0.571	
OWB_2	X-20-1	1,061	1,009	1,033	731	1,109	850	1.880	1.547
	X-20-6	1,111	1,067	1,049	757	1,147	853	2.408	1.342
	X-20-9	1,127	1,077	1,091	743	1,111	866	1.608	1.067
	X-20-11	1,121	1,068	1,098	797	1,182	827	2.159	1.332

LREE contents than D/HZ/L clinopyroxene from sample X-6, but due to apparently lower HREE, they show the most fractionated La_N/Lu_N ratios, in the range 8–21. Sample BT-2 from the Massif Central (Mason et al. 1999) displays a roughly similar chondrite-normalized trace element pattern. It is also characterised by a distinctive Sr peak and similar REE contents and ratios.

Coarse clinopyroxene crystals in the Cpx-L, those occurring in OWB_1 xenoliths and Cpx-M all have similar chondrite-normalized trace element patterns shown in Fig. 11C–E. They display a slightly concave downward pattern, with moderately fractionated REE (La_N/Lu_N mostly between 2 and 4). Cpx from Cpx-L generally have La_N/Ce_N ratios <1. Those from Cpx-L show slightly flatter HREE slopes ($Dy_N/Lu_N \sim 1.5$) than clinopyroxene from OWB_1 ($Dy_N/Lu_N \sim 2$) and megacrysts ($Dy_N/Lu_N \sim 3$). However, in contrast to both interstitial and pocket cpx from D/HZ/L samples, they all show large troughs at both Zr–Hf and Nb–Ta, and smaller troughs at Sr and Y. Trace element compositions of vein cpx from the Eifel (Witt-Eickschen and Kramm 1998) and megacrysts from the Pannonian Basin (Dobosi and Jenner 1999; Dobosi et al. 2003) are also shown in Fig. 11C–E. They show remarkably similar patterns to cpx occurring in Cpx-L and OWB_1 mantle xenoliths and megacrysts from East Serbia. The similarity is especially obvious when comparing megacryst populations from the Pannonian Basin and East Serbia. The shape of the spider diagram is completely parallel with only slightly higher concentrations of all trace elements in the Serbian megacrysts, suggesting a similar origin.

Discussion

Textural evidence and chemical composition of minerals in the Serbian mantle xenoliths provide some important constraints on characteristics of lithospheric upper mantle beneath this part of Europe. In this context, we can distinguish between (a) ‘primary’ features that are characteristic of the main mantle mineralogy and processes responsible for equilibration of the major phases, and (b) ‘secondary’ characteristics that include effects of various metasomatic processes. The former aspect will be discussed on the basis of protogranular or slightly deformed D/HZ/L xenoliths, which form the most abundant mantle lithology. The latter is related to the presence of Cpx-L and OWB xenoliths and Cpx-M. It may be significant that the southern locality (Striževac) contains only D/HZ/L xenoliths (some of which contain secondary pockets and veinlets) and very rare Cpx-M, and all the variety of other lithologies (Cpx-L, both OWB_1 and OWB_2 and Cpx-M) are found only in Sokobanja in the north. This might be related to the position of Sokobanja which is situated much closer to the subduction-related Late Cretaceous volcanics of the Timok Magmatic Complex (Fig. 1). Hence, Sokobanja basanites might have sampled the lithosphere which had been previously more affected by subduction processes.

Main characteristics of the East Serbian lithospheric mantle

Textural characteristics, modal composition and major element contents and ratios in the constituent minerals suggest that the protogranular D/HZ/L xenoliths most likely represent the predominant lithology in the lithospheric mantle. They are analogous to the type I of Frey and Prinz (1978) or Menzies (1983). Estimates of oxygen fugacity for the D/HZ/L xenoliths between -0.5 and $+1.8$ $\log(fO_2)$ units relative to the FMQ buffer (ΔFMQ) may reflect the values within the "normal" lithosphere beneath East Serbia. In addition, Fe–Mg distribution between coexisting olivines and opx (Fig. 7) indicates very good equilibration and the olivine-spinel "mantle array" (Fig. 5) shows that the D/HZ/L xenoliths fall within the field of typical mantle. They are most probably related to depletion via extraction of basaltic melt, particularly indicated by the Mg# vs. Al_2O_3 (wt%) variations in opx (Fig. 6) and Cr–Al trends in coarse spinels (Fig. 9).

In order to discuss mantle depletion processes, whole-rock abundances of major oxides have been recalculated using mass-balance calculations based on mineral chemistry and modal composition of the xenoliths. Figure 12 presents variation plots of whole-rock MgO contents vs. CaO, Al_2O_3 and TiO_2 using the calculated wt%. The calculated composition of the East Serbian xenoliths is consistent within scatter with trends seen worldwide, for instance they plot within the fields of chemical composition of European mantle xenoliths and ultramafic massifs (Downes 2001). Most Serbian D/HZ/L xenoliths plot within the fields, although occupying the most depleted end of each array, suggesting that the Serbian mantle is more depleted than typical European Mantle. The high degree of depletion is in keeping with very low modal content of clinopyroxene and that is in accordance with low Na_2O (wt%) in clinopyroxene and Al_2O_3 (wt%) in orthopyroxene.

In terms of trace elements, however, cpx from harzburgite X-6 do not show LREE-depleted compositions (Fig. 11A). Instead, they show a general increase in chondrite-normalised concentrations from the more compatible HREE (10× chondrite) to the most incompatible LREE (100× chondrite). Even high field strength elements such as Nb and Ta are enriched in these cpx, although minor troughs are present at Zr and Hf. A similar Zr–Hf trough is shown by sample RP 83-72 from the Massif Central, which is interpreted as a harzburgite previously depleted by basaltic melt extraction that has been cryptically metasomatised by LREE-rich fluids (Mason et al. 1999). However, X-6 cpx display overall higher HREE contents and that may imply that even this clinopyroxene does not represent a primary phase of a restitic mantle, but a product of metasomatism caused by percolation of alkaline magma. The lack of true HREE depleted trace element patterns in Serbian xenoliths may be simply due to insufficient data, as only one interstitial clinopyroxene from D/HZ/L xenoliths

Table 8 Representative LA-ICP-MS analyses of clinopyroxenes from East Serbian mantle xenoliths

	D/HZ/L (X-6)			P and V (Sb-4)					Cpx-rich L (X-1)			Cpx-L (X-11/1)				OWB_1 (Sb-3)			M (K-8)	
	Cpx1	Cpx2	Cpx3	Cpx1	Cpx2	Cpx3	Cpx4	Cpx5	Cpx1	Cpx2	Cpx3	Cpx1	Cpx2	Cpx3	Cpx4	Cpx1	Cpx2	Cpx3	Cpx1	Cpx2
Nb	25.24	10.57	17.31	56.56	10.61	24.08	12.18	4.47	5.80	2.30	2.70	0.26	1.01	0.34	0.18	1.49	1.50	1.14	0.53	0.52
Ta	1.55	0.70	1.44	3.36	0.88	1.77	1.24	0.19	0.25	0.17	0.14	0.08	0.08	0.05	0.07	0.23	0.08	0.34	0.14	0.14
La	22.32	21.90	16.38	29.76	15.79	20.83	13.65	6.01	10.84	3.69	4.84	3.06	4.08	3.33	4.47	10.52	9.07	8.13	3.80	4.69
Ce	41.52	76.43	45.87	55.03	25.62	41.45	23.04	12.90	23.71	13.17	12.29	12.06	12.53	12.81	13.36	32.93	31.91	30.35	15.48	17.18
Pr	6.88	6.23	7.56	5.43	2.41	4.77	2.60	1.42	4.05	2.39	2.15	2.22	2.35	2.15	2.31	5.91	5.72	6.35	2.23	3.17
Sr	379.21	278.97	263.37	678.46	1358.81	622.10	832.42	209.81	162.82	172.31	111.71	134.66	131.55	130.43	143.10	438.88	432.52	365.79	118.02	127.63
Nd	24.75	34.32	29.35	17.01	9.03	16.64	8.22	4.86	18.60	13.66	10.75	12.39	10.62	10.81	12.94	29.67	30.19	31.26	15.05	17.96
Sm	7.64	7.39	6.64	3.62	0.80	2.82	1.72	1.14	7.26	5.46	4.24	4.88	3.27	3.46	5.32	8.58	7.80	8.60	5.61	6.64
Zr	63.95	58.71	80.01	97.50	45.93	67.56	52.50	28.87	60.06	36.82	32.29	15.69	20.10	19.48	22.67	97.13	85.41	62.62	42.77	44.99
Hf	2.62	1.96	2.87	2.72	1.43	3.08	2.17	2.21	1.61	0.33	0.65	0.69	0.95	0.57	0.91	2.70	3.09	3.97	2.47	2.83
Eu	2.19	2.25	2.35	1.22	0.49	0.67	0.71	0.16	2.30	2.03	1.44	1.31	0.98	1.04	1.51	2.93	2.74	2.86	1.78	2.04
Gd	7.39	4.94	7.29	2.74	1.06	2.23	0.88	1.15	4.98	3.58	2.85	4.42	3.09	1.98	3.49	7.14	5.66	5.76	4.98	4.73
Tb	1.40	0.82	1.13	0.42	0.19	0.29	0.17	0.15	0.54	0.35	0.30	0.61	0.44	0.39	0.65	0.95	0.99	1.27	0.79	0.97
Dy	3.61	4.17	5.38	2.14	0.88	1.85	1.41	0.35	4.55	2.44	2.33	2.77	2.73	2.61	3.48	5.53	5.42	6.51	5.34	5.37
Y	16.63	16.37	18.28	10.20	4.87	7.78	4.95	3.40	27.05	15.44	14.16	13.97	10.31	9.90	11.87	25.38	24.11	19.54	16.90	18.68
Ho	1.25	0.72	0.93	0.45	0.26	0.39	0.39	0.21	1.06	0.75	0.60	0.77	0.38	0.69	0.71	1.18	1.05	1.51	0.88	0.92
Er	1.14	1.08	1.78	1.85	0.98	0.74	0.79	0.59	2.01	1.19	1.07	1.96	1.23	1.27	1.43	2.37	2.62	3.33	2.53	3.35
Tm	0.21	0.48	0.48	0.14	0.09	0.20	0.09	0.12	0.39	0.38	0.26	0.18	0.18	0.31	0.27	0.28	0.35	0.55	0.29	0.26
Yb	1.05	2.87	2.09	1.84	0.58	1.52	1.17	0.45	2.34	1.00	1.11	1.72	1.39	1.42	1.21	1.95	1.76	2.19	1.96	1.77
Lu	0.27	0.27	0.21	0.17	0.12	0.25	0.18	0.03	0.37	0.25	0.21	0.16	0.16	0.25	0.14	0.24	0.34	0.29	0.17	0.08

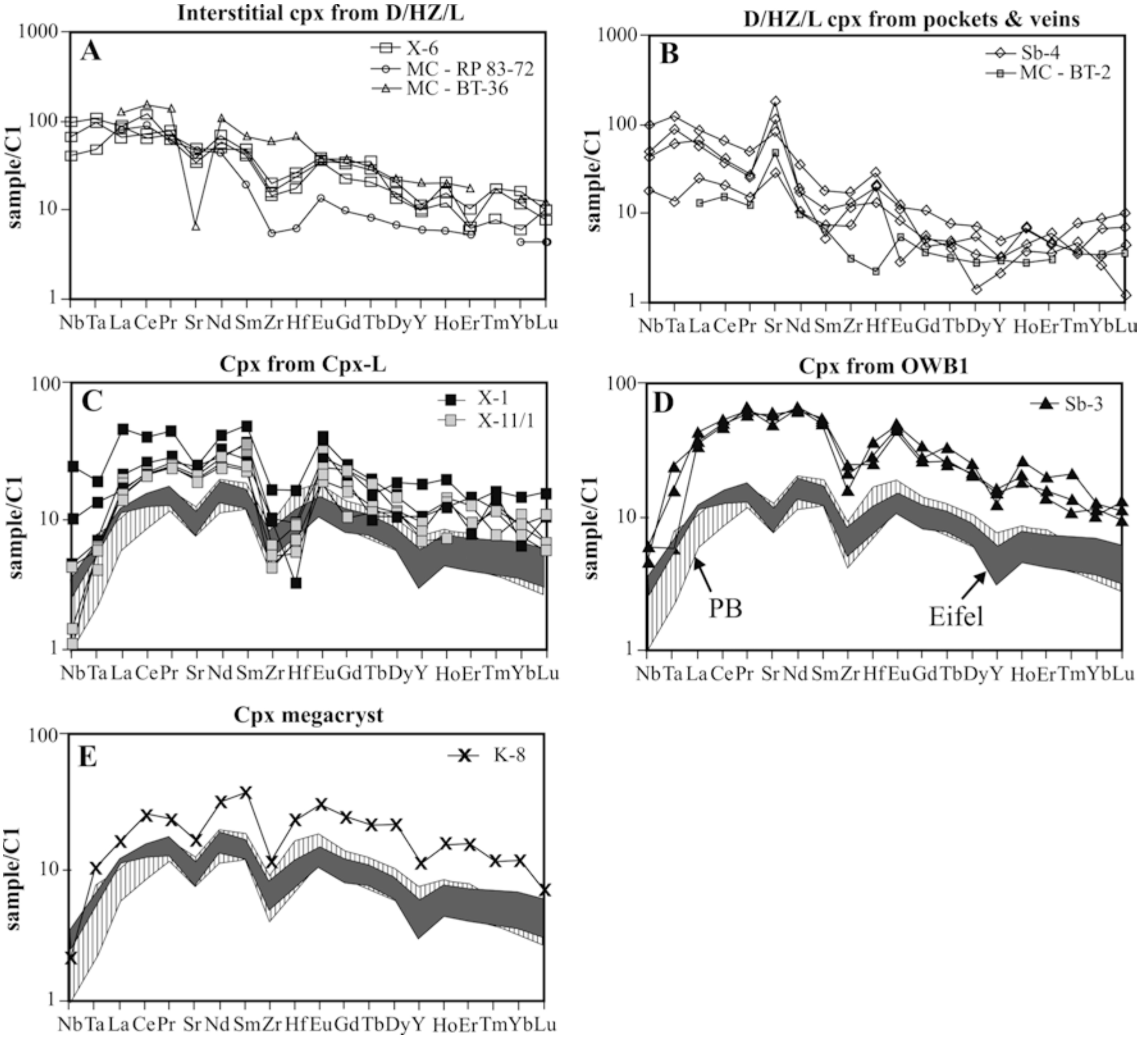

Fig. 11A–E Chondrite-normalized trace element contents of clinopyroxene from **A** D/HZ/L (interstitial), **B** D/HZ/L (pockets and veins), **C** Cpx-L, **D** OWB_1 **E** Cpx-M; clinopyroxenes from East Serbian xenoliths are compared with clinopyroxenes in xenoliths from Massif Central (MC-RP-83-72, MC-BT-36 and MC-BT-2 after Mason et al. 1999), Eifel (Witt-Eickschen and Kramm 1998) and clinopyroxene megacrysts from the Pannonian Basin (*PB* Dobosi et al. 2003); normalization on C1-chondrite from Sun and McDonough (1989)

was analysed. In this context, the origin of low-Al orthopyroxene is also difficult to interpret. They may simply reflect a higher degree of depletion within the East Serbian mantle, but also they may have formed via hydrous metasomatic processes usually related to subduction. The latter model is closely related to the presumed origin of OWB_2 xenoliths (see below).

Only the highest temperature estimates for D/HZ/L xenoliths approach the geotherms of the Styrian Basin and Persani Mts (Sachsenhofer et al. 1997; Lankreijer et al. 1997; Falus et al. 2000). These are small basins belonging to the neighbouring Pannonian area, which is generally characterized by a high surface heat flow (~100 mW/m^2; Pollack and Chapman 1977) and thin lithosphere of <60 km (Ádám et al. 1989). During the formation of Palaeogene alkaline magmatism in East Serbia, conditions were therefore characterized by lower heat flow and thicker lithosphere.

Origin of Cpx-L, spinel-rich OWB_1 xenoliths and Cpx-M

Clinopyroxene-rich lherzotites, OWB_1 and Cpx-M are characterized by extremely fertile compositions. Their olivine and orthopyroxene (when present) display relatively low Mg# (<89). Orthopyroxene and clinopyroxene show high Al_2O_3 and TiO_2 and lower Cr_2O_3 contents compared to the minerals from the D/HZ/L xenoliths. These characteristics indicate that these xenoliths cannot be regarded as 'normal' upper mantle. Instead, they are likely related to magmatic modifications of the upper mantle (e.g. McGuire and Mukasa 1997; Griffin et al. 1999). Similar trace element patterns for cpx in the Cpx-L and OWB_1 xenoliths and megacryst clinopyroxene (Fig. 11) suggest a common origin for these three lithologies. They all show slightly to distinctively concave downward REE patterns and HFSE depletion.

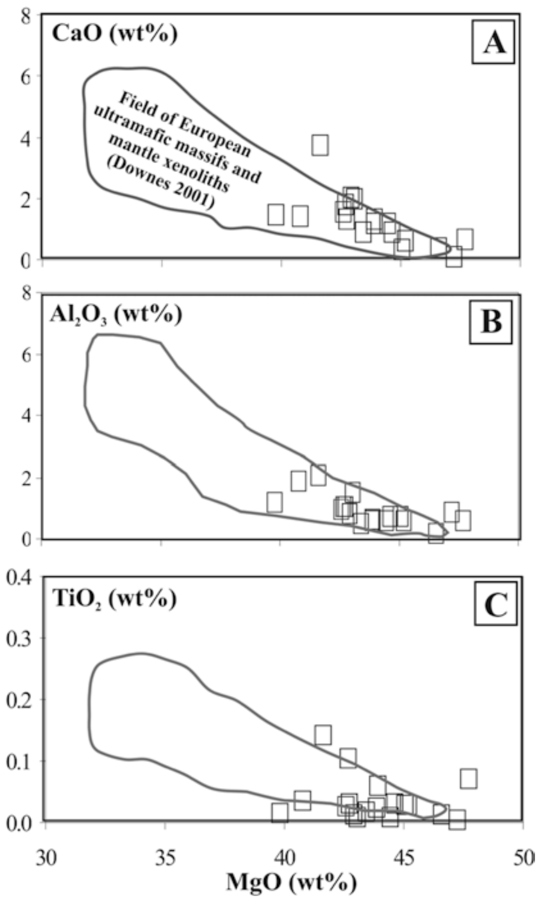

Fig. 12A–C MgO vs. CaO (wt%) (**A**), MgO vs. Al_2O_3 (wt%) (**B**) and MgO vs. TiO_2 (wt%) (**C**) variation diagrams for D/HZ/L East Serbian mantle xenoliths. Major element composition for the xenoliths calculated on the basis of modal mineral contents and mineral chemistry (see explanation in the text); fields of the oxide variations for mantle xenoliths and ultramafic massifs from Europe according to Downes (2001)

Clinopyroxene megacrysts are often found in alkaline basalts. They have been proposed as part of the Al-augite series of Wilshire and Shervais (1975) or type II xenoliths (Frey and Prinz 1978). Usually, they are interpreted in terms of cognate crystals from the alkaline magma (e.g. Binns et al. 1970) or as fragments of pegmatitic rocks crystallized from basaltic magma within the subcontinental lithosphere (e.g. Irving 1974; Shaw and Eyzaguirre 2000). East Serbian Cpx-M show compositional similarities to vein cpx of the Eifel district (Witt-Eickschen and Kramm 1998), and to Cpx-M entrained in Pliocene alkaline basalts of the western Pannonian Basin. For the latter, Dobosi et al. (2003) presented evidence to suggest that they originated via earlier intrusions of alkaline mafic magmas into the base of the lithosphere.

In order to calculate the trace element composition of a melt which could have co-existed with the Cpx-M, as well as with clinopyroxene occurring in Cpx-L and OWB_1, we have used cpx/melt partition coefficients reported by Downes et al. (2004a) and Vannucci et al. (1998). Figure 13 shows calculated chondrite-normalized trace element abundances of melts in equilibrium with the studied cpx. Normalized trace element patterns are compared with those three samples of Sokobanja basanites (Jovanović et al. 2001). It is obvious that the liquid composition calculated on the basis of trace element concentration in the clinopyroxene megacryst (K-8), using partition coefficients after Downes et al. (2004a), matches very well the pattern of basanites, although the calculated pattern has slightly lower Nb and Zr contents. The liquid composition estimated on the basis of $^{cpx/melt}$ Ds of Vannucci et al. (1998) differs from the basanites in its lower La and Ce contents, and in having a pronounced trough at Zr. Similarly, liquid compositions based on cpx from Cpx-L and OWB_1 show a similar pattern to the Sokobanja basanites and, again, closer agreement has been obtained using $^{cpx/melt}$ Ds of Downes et al. (2004a). In contrast to the liquid in equilibrium with the clinopyroxene megacryst, these estimates differ in significantly lower Zr contents. Thermometric calculations showed that OWB_1 xenoliths have attained thermal and chemical equilibrium. Therefore it is possible that subsolidus equilibrium would also affect partitioning of trace elements between co-existing minerals, i.e. that negative HFSE anomalies in clinopyroxene are compensated by positive HFSE anomalies in orthopyroxene (e.g. Bedini and Bodinier 1999). In this context it might be not appropriate to estimate the trace element composition of parental melts using cpx analyses, at least for OWB_1 xenoliths, in which orthopyroxene is far more abundant than clinopyroxene. On the other hand, there is apparent similarity in the overall trace element pattern between OWB_1 clinopyroxenes and those clinopyroxenes occurring as the dominant phase (Cpx-L) or as megacrysts.

The similarity of calculated trace element compositions to Sokobanja basanites suggests that the supposed metasomatic agents are likely genetically and compositionally akin to mafic alkaline melts. The similarity between patterns of the liquid calculated from clinopyroxene megacryst (K-8) and the host basanites is to be expected, since megacrysts are usually explained as direct precipitates from similar alkaline melts (e.g. Aoki and Kushiro 1968; Irving 1974; Wilshire and Shervais 1975; Dal Negro et al. 1989; Righter and Carmichael 1993; Dobosi and Jenner 1999; Shaw and Eyzaguirre 2000; Brizi et al. 2003; Dobosi et al. 2003). Differences displayed by calculated liquid compositions which equilibrated with cpx from Cpx-L and OWB_1 could be due to reactions with pre-existing mineral assemblages rather than direct crystallization from the infiltrating alkaline melt. However, if we relate the genesis of OWB_1 mantle lithology to the activity of alkaline melts within the lithosphere, their modal orthopyroxene-rich nature is problematic. The OWB_1 xenoliths could have originated as a specific orthopyroxene-rich mantle lithology (e.g. olivine orthopyroxenite?), which subsequently underwent modal metasomatism caused by alkaline mafic melts and crystallization of clinopyroxene. However, the origin of this opx-rich mantle remains an open question. A possible explanation that this opx-rich mantle material originated as OWB_2 xenoliths (see below) is not likely, given the textural and compositional differences between pyroxenes and especially spinels occurring in OWB_1 and OWB_2 xenoliths.

Metasomatic processes and the formation of pockets and veinlets

Clinopyroxene-bearing pockets and veinlets are relatively common in D/HZ/L xenoliths from both localities in Serbia. Similar pockets and veinlets are reported in xenoliths from many other localities (Frey and Green 1974; Edgar et al. 1989; Schiano et al. 1995; Zinngrebbe and Foley 1995; Szabó et al. 1996; Wulff-Pedersen et al. 1996; Bali et al. 2002). Based on textural relationships and diffusion experiments, they have mostly been interpreted as products of in situ reactions in the upper mantle (Ionov et al. 1994; Zinngrebbe and Foley 1995; Wulff-Pedersen et al. 1996, 1999; Ionov et al. 1999; Dawson 2002). In contrast, Shaw (1999) argued that at least some of these assemblages could have resulted from reactions with the host magma.

Mineral chemistry and textural relationships of reactions observed in the Serbian xenoliths lend support to the hypothesis that most pockets and veinlets originated in response to metasomatic processes in the upper mantle. The first approach is to compare the reactions presumed to have occurred in the mantle and those obviously formed within the host basanite. Reaction selvages produced by orthopyroxene replacement at the edges of the xenoliths form perpendicularly oriented olivine + glass simplectites. This suggests rapid quench-like reactions during which further orthopyroxene dissolution was prevented by nucleation of clinopyroxene phenocrysts from the basanite groundmass (Fig. 3G). A similar reaction pattern was suggested by Klügel (2001) on the basis of Fe–Mg interdiffusion rates of orthopyroxene from Canary Islands xenoliths. The predominance of olivine in these selvages is consistent with the 0.4 GPa orthopyroxene dissolution experiments of Shaw (1999).

Compared with the assemblages observed at the orthopyroxene-basanite interface, the replacement of orthopyroxene crystals deep within xenoliths is clearly different. The reaction product is almost exclusively clinopyroxene whereas olivine is mostly absent (Fig. 3F). This is in accordance with high-pressure dissolution experiments (Shaw 1999), which suggested shrinking of the olivine stability field with increasing pressure. Moreover, the reactions presumed to have occurred in situ display transitions from clinopyroxene-rimmed orthopyroxene through larger clinopyroxene grains enclosing orthopyroxene relics (visible only in BSE images, e.g. Fig. 3E) to irregular clinopyroxene-pockets free of orthopyroxene (Fig. 3C, D). Conditions for such reactions probably require a much longer time than the estimated eruption time of xenolith-bearing alkali magmas [< 100 h, according to Kushiro (1976), Mercier (1979) and O'Reilly (1989].

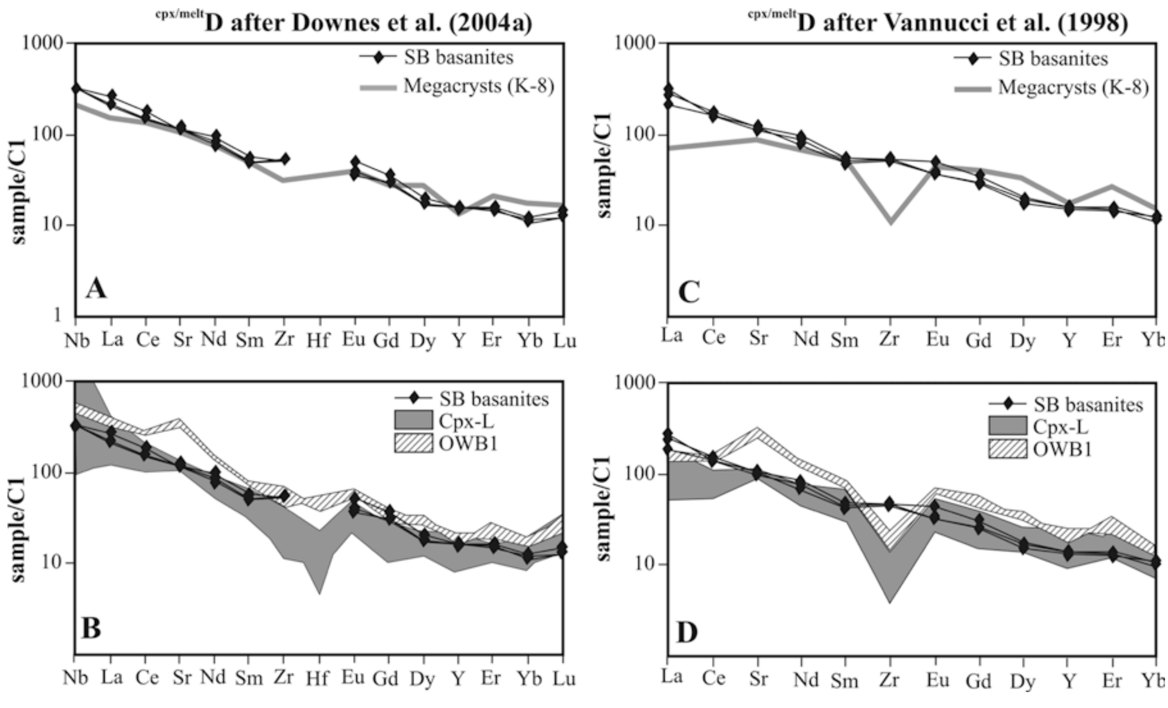

Fig. 13A–D Chondrite normalized trace element contents of metasomatic liquid which was calculated to have been in equilibrium with clinopyroxene from Cpx-rich L and OWB_1 (**A, B**) and clinopyroxene megacryst (**C, D**); Cpx/melt partition coefficients reported from Vannucci et al. (1998) and Downes et al. (2004a) have been used and for comparison the trace element pattern of three samples of Sokobanja basanites are presented (Jovanović et al. 2001)

Textural and mineralogical characteristics of the pockets in the D/HZ/L xenoliths that also suggest a metasomatic origin can be summarized as follows: (a) they are commonly situated inside xenoliths, (b) when located at the periphery they display sharp contacts with the groundmass, (c) elongated pockets/stringers are oriented subparallel to the longer axis of the xenolith, (d) euhedral cpx within pockets are usually subparallel (Fig. 3D), (e) the clinopyroxene is Cr-rich greenish diopside generally interpreted to be of sub-Moho origin and (f) transitions from clinopyroxene-glass ($\pm$olivine) intergrowths to coarser spongy clinopyroxene indicate different stages of a similar reaction.

The genesis of glass-bearing pockets and veinlets in mantle xenoliths has been variously explained. They have been interpreted by infiltration-reaction-crystallization models (e.g. Edgar et al. 1989; Schiano et al. 1995; Zinngrebe and Foley 1995; Wulff-Pedersen et al. 1996, 1999; Coltorti et al. 1999), decompression breakdown of hydrous phases (e.g. Frey and Green 1974; Francis 1976), immiscibility of melts (Schiano et al. 1994) and in situ melting processes (Amundsen 1987; Francis 1987; Hauri et al. 1993; Ionov et al. 1994; Chazot et al. 1996). Numerous replacement features and dissolution/reaction relationships observed within the pockets and veins tend to support infiltration models, suggesting an AFC-type reaction between a metasomatic agent and wall-rock spinel peridotite (e.g. Kelemen 1990). The occurrence of glass and feldspar within some pockets indicates that metasomatism probably occurred shortly before the xenoliths were captured by the alkaline magma. This may imply that the metasomatic agent was temporally and probably genetically related to the basanitic magmatism. Silicate melt pockets in upper mantle xenoliths of the Pannonian Basin were interpreted as the result of subduction metasomatism (Bali et al. 2002). They contain similar mineral phases as pocket and vein assemblages of East Serbian D/HZ/L xenoliths, but strongly differ in the very high Mg# s of their silicate phases and very low TiO_2 contents of spinels (up to 0.6 wt%) which implies a different origin than melt pockets within Serbian D/HZ/L xenoliths.

The pocket cpx display the most fractionated REE pattern (La_N/Ce_N around 2, La_N/Lu_N up to 21) in comparison to all other cpx (La/CeN/Lu_N up to 9). In order to calculate a possible composition of metasomatic melts that caused metasomatism we have used partition coefficients reported by Downes et al. (2004a). Chondrite-normalized calculated trace element contents of liquids in equilibrium with clinopyroxene from a pocket (sample Sb-4) are shown in Fig. 14, together with the trace element pattern of the host basanites (Jovanović et al. 2001). The overall patterns are only roughly similar, but the calculated metasomatic liquids have much more fractionated LREE/HREE (La_N–Lu_N up to 90) and MREE/HREE (La_N–Sm_N mostly around 30). They also have a distinctive positive anomaly at Sr. In addition, the supposed liquid appears to be very rich in Nb (above 1,000× chondrite). The inferred affinity of

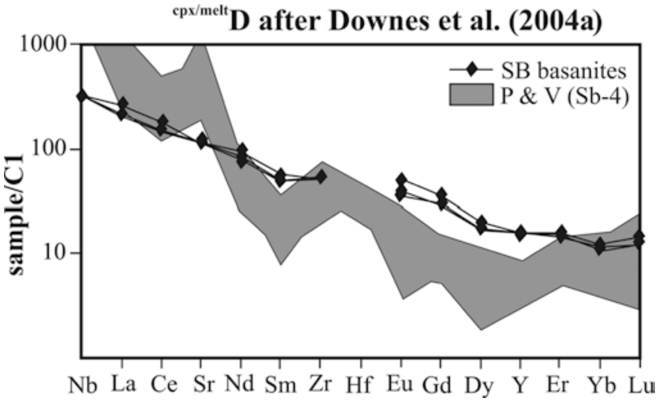

Fig. 14 Chondrite-normalized trace element contents of calculated composition of metasomatic liquid in equilibrium with clinopyroxene from pockets and veins in D/HZ/L xenoliths. Cpx/melt partition coefficients are from Downes et al. (2004a) and for comparison the trace element pattern of three samples of Sokobanja basanites are presented (Jovanović et al. 2001)

these melts should be regarded with caution, given that relationships between liquid composition, structure and crystal chemical controls are not well known. Factors such as degree of polymerization of melts, crystal structure of clinopyroxene and crystallization of co-existing minerals (apatite, Ti-rich spinel, etc.) could have important effects on $^{cpx/melt}$ Ds, especially for Sr (e.g. Vannucci et al. 1998). Although some inconsistencies of this model arise from the lack of reliable information about the composition of the glass co-existing with clinopyroxene in the pockets, we argue that the metasomatic fluids were also genetically related to alkaline mafic magma. The Fe–Ti enrichment trend of spinel reactions found in pockets and veins and the presence of a Ti-rich phlogopite flake support this hypothesis.

Origin of spinel-poor olivine-websterite xenoliths (OWB_2)

Spinel-poor olivine websterite xenoliths are extremely orthopyroxene-rich and fall outside the main compositional trends of the D/HZ/L suite. Their silicate minerals are also iron-rich in comparison to those in the D/HZ/L samples. Spinels in OWB_2 show a strong affinity to oxides formed by the crystallisation of mafic and ultramafic magma rather than those found in mantle peridotites (Fig. 10A). On the basis of the Cr_2O_3 (wt%) vs. Al_2O_3 (wt%) diagram they are akin to magmatic spinels (Conrad and Kay 1984) (Fig. 10B). These characteristics argue that they represent a separate subordinate lithology within the East Serbian lithosphere, probably resulting from percolation of mafic/ultramafic magma (but not related to the alkaline host). This is supported by textural evidence such as the appearance of euhedral olivine crystals which usually crystallize from melts.

There is evidence that the source for the OWB_2 melt might have been generated in a highly refractory mantle. This can be inferred from the very low Al_2O_3 and TiO_2

contents in co-existing orthopyroxene and clinopyroxene, coupled with extremely high Cr#s in spinel (Fig. 9). Such extraordinary Cr-rich spinels are found mainly in boninites and other arc-related magmas (e.g. Barnes and Roeder 2001). McInnes et al. (2001) have attributed the presence of analogous Al-depleted and Cr-rich spinels from Lihir (Papua New Guinea) to a hydrous metasomatism of oceanic sub-arc mantle. The presence of an interstitial mineral association dominated by K-feldspar (± plagioclase) indicates that the interstitial melt was Si-rich. Along with relatively high oxygen fugacity estimates (1–2.4 log units above the FMQ buffer), this suggests that the magma that gave rise to the OWB_2 lithology probably originated from flux-induced melting of a refractory mantle source, suggesting a subduction setting.

The generation of OWB_2 mantle lithology within the East Serbian lithosphere may be related to tectonic processes that had occurred before the Palaeogene alkaline magmatism. Late Cretaceous eastward/northeastward subduction of Tethyan oceanic lithosphere beneath stable Europe (e.g. Ianovici et al. 1977; Karamata et al. 1997) was likely responsible for OWB_2 formation. The same subduction events could have produced mafic/ultramafic melts which precipitated within the cold mantle in the fore-arc region which matches the line where Palaeogene mafic alkaline rocks of East Serbia occur (Fig. 1).

Concluding remarks

East Serbian Palaeogene mafic alkaline rocks contain various mantle xenoliths and xenocrysts, which help us to better understand characteristics of the lithosphere beneath Southeast Europe, as well as to explain some aspects of the Mesozoic and Cainozoic mantle dynamics in this region.

Dunite/harzburgite/lherzolite xenoliths show that the East Serbian subcontinental mantle is mainly harzburgitic, recording previous processes of extraction of basaltic melts. A rather high degree of depletion is inferred from modal mineral composition, mineral chemistry and recalculated whole-rock major element contents. However, this is not apparent from the trace element contents in cpx, which do not seem to reflect previous depletion processes. The highest temperature estimates approach the geotherms of the Styrian Basin and Persani Mts. Re-fertilization and formation of clinopyroxene-rich domains in the lithosphere occurred in response to infiltration of alkali melts, genetically and compositionally related to the host basanite magma. The same appears to be valid for numerous pockets and veins found in the D/HZ/L xenoliths. The differences in lithology of these xenoliths may be related to a possibility that pockets and veins are products of reactions in their incipient stages, Cpx-L and OWB_1 are much better equilibrated, whereas clinopyroxene ± olivine megacrysts may represent fragments of deep-seated high-pressure cumulates of alkali mafic magma. Some compositional variations of the existing minerals were likely produced by slight changes in composition of metasomatic agents, level of percolation, duration of reactions and degree of equilibration.

The generation of OWB_2 xenoliths is probably related to the Cretaceous subduction processes and magmatism and may have crystallized from mafic/ultramafic and related magmas.

Acknowledgements Principal funding for this study was provided by a Joint Project Grant of the British Royal Society (UK). We are grateful to Andy Beard for his assistance with the microprobe analyses and Bill Perkins (University of Aberystwyth) for help with LA-ICP-MS data. Constructive reviews of D. Bell and Y.Xu are appreciated. V.C. and D.P. acknowledge the support of the Ministry of Science, Technology and Development of Republic of Serbia, Project no. 1767.

References

Ádám A, Nagy Z, Varga G (1989) Magnetotelluric (MT) research and exploration in Hungary. Geophysics 54:795–797

Amundsen HEF (1987) Peridotite xenoliths from Gran Canaria, Canary Islands; evidence for metasomatic processes and partial melting in the lower oceanic crust. Neues Jahrb Mineral Abh 156:121–140

Aoki K, Kushiro I (1968) Some clinopyroxenes from ultramafic inclusions in Dreiser Weiher, Eifel. Contrib Mineral Petrol 25:284–288

Arai S (1994) Characterization of spinel peridotites by olivine-spinel compositional relationships: review and interpretation. Chem Geol 113:191–204

Bali E, Szabó Cs, Vaselli O, Török K (2002) Significance of silicate melt pockets in upper mantle xenoliths from the Bakony-Balaton highland volcanic field, Western Hungary. Lithos 61:79–102

Ballhaus C, Berry RF, Green DH (1991) High pressure experimental calibration of the olivine-orthopyroxene-spinel oxygen geobarometer: implication for the oxidation state of the upper mantle. Contrib Mineral Petrol 107:27–40

Barnes SJ, Roeder PL (2001) The range of spinel composition in terrestrial mafic and ultramafic rocks. J Petrol 42(12):2279–2302

Bedini RM, Bodinier J-L (1999) Distribution of incompatible elements between the constituents of spinel peridotite xenoliths: ICP-MS data from the East African rift. Geochim Cosmochim Acta 63(122):3883–3900

Binns RA, Duggan MB, Wilkinson JFG, Kalocsai GIZ (1970) High pressure megacrysts in alkaline lavas from northeastern New South Wales. Am J Sci 269:132–168

Brey GP, Kohler TP (1990) Geothermobarometry in four phases lherzolites II. New thermobarometers and practical assessment of existing thermobarometers. J Petrol 31:1353–1378

Brizi E, Nazzareni S, Princivalle F, Zanazzi PF (2003) Clinopyroxenes from mantle-related xenocrysts in alkaline basalts from Hannuoba (China): augite-pigeonite exsolutions and their thermal significance. Contrib Mineral Petrol 145:578–584

Chazot G, Menzies MA, Harte B (1996) Determination of partition coefficients between apatite, clinopyroxene, amphibole, and melt in natural lherzolites from Yemen: implications for wet melting in the lithospheric mantle. Geochim Cosmochim Acta 60:423–437

Coltorti M, Bonadiman C, Hinton RW, Siena F, Upton BGJ (1999) Carbonatite metasomatism of the oceanic upper mantle: evidence from clinopyroxenes and glasses in ultramafic xenoliths of Grande Comore, Indian Ocean. J Petrol 40:133–165

Conrad WK, Kay RW (1984) Ultramafic and mafic inclusions from Adak Island: crystallisation history and implications for the nature of primary magmas and crustal evolution in the Aleutian arc. J Petrol 25:88–125

Cvetković V, Downes H, Prelević D, Jovanović M, Vaselli O (2001) Sokobanja mantle xenoliths and megacrysts—the first insight into the East Serbian lithospheric Mantle. In: Pancardi meeting 2001, Sopron, DO-5

Cvetković V, Prelević D, Downes H, Jovanović M, Vaselli O, Pécskay Z (2004) Origin and geodynamic significance of tertiary post-collisional basaltic magmatism in Serbia (central Balkan Peninsula). Lithos 73(3–4):161–186

Dal Negro A, Manoli S, Secco L, Piccirillo EM (1989) Megacrystic clinopyroxenes from Victoria (Australia): crystal chemical comparisons of pyroxenes from high and low pressure regimes. Eur J Miner 1:105–121

Dawson JB (2002) Metasomatism and partial melting in upper-mantle peridotite xenoliths from the Lashaine Volcano, Northern Tanzania. J Petrol 43(9):1749–1777

Dick HJB, Bullen T (1984) Chromian spinel as petrogenetic indicator in abyssal and alpine-type peridotites and spatially associated lavas. Contrib Mineral Petrol 86:54–76

Dobosi G, Jenner GJ (1999) Petrologic implications of trace element variation in clinopyroxene megacrysts from the Nógrád volcanic province, north Hungary: a study by laser ablation microprobe–inductively coupled plasma-mass spectrometry. Lithos 46:731–749

Dobosi G, Downes H, Embey-Isztin A, Jenner G (2003) Origin of megacrysts and pyroxenite xenoliths from the Pliocene alkali basalts of the Pannonian Basin (Hungary). Neues Jahrb Miner Abh 178:217–237

Downes H (2001) Formation and modification of the shallow sub-continental lithospheric mantle: a review of geochemical evidence from ultramafic xenolith suites and tectonically emplaced ultramafic massifs of Western and Central Europe. J Petrol 42:233–250

Downes H, Embey-Isztin A, Thirlwall M (1992) Petrology and geochemistry of spinel-peridotite xenoliths from the western Pannonian Basin (Hungary): evidence for an association between enrichment and texture in the upper mantle. Contrib Mineral Petrol 107:340–354

Downes H, Vaselli O, Seghedi I, Ingram G, Rex D, Coradossi D, Pécskay Z, Pinarelli L (1995) Geochemistry of late Cretaceous-early Tertiary magmatism in Poiana Rusca (Romania). Acta Volcanol 7(2):209–217

Downes H, Beard A, Hinton R (2004a) Natural experimental charges: an ion-microprobe study of trace element distribution coefficients in glass-rich hornblendite and clinopyroxenite xenoliths. Lithos 75(1–2):1–17

Downes H, Macdonald R, Upton BGJ, Cox KG, Bodinier J-L, Mason PRD, James D, Hill PG, Hearn BC (2004b) Ultramafic xenoliths from the Bearpaw Mountains, Montana, USA: evidence for multiple metasomatic events in the lithospheric mantle beneath the Wyoming craton. J Petrol (in press)

Edgar AD, Lloyd FE, Forsyth DM, Barnett RL (1989) Origin of glass in upper mantle xenoliths from the Quaternary volcanics of Gees, West Eifel, Germany. Contrib Mineral Petrol 133:277–286

Embey-Isztin A, Scharbert HG, Dietrich H, Poultidis H (1989) Petrology and geochemistry of peridotite xenoliths in alkali basalts from the Transdanubian volcanic region. J Petrol 30:79–106

Embey-Isztin A, Dobosi G, Altherr R, Meyer HP (2001) Thermal evolution of the lithosphere beneath the western Pannonian Basin: evidence from deep-seated xenoliths. Tectonophysics 331:285–306

Falus Gy, Szabó Cs, Vaselli O (2000) Mantle upwelling within the Pannonian Basin: evidence from xenolith lithology and mineral chemistry. Terra Nova 12:295–302

Francis DM (1976) The origin of amphibole in the lherzolite xenoliths from Nunivak Island, Alaska. J Petrol 17:357–378

Francis DM (1987) Mantle-melt interaction recorded in spinel lherzolite xenoliths from the alligator lake volcanic complex, Yukon, Canada. J Petrol 28:569–597

Frey FA, Green DH (1974) The mineralogy, geochemistry and origin of lherzolite inclusions in Victoria basanites. Geochim Cosmochim Acta 38:1023–1059

Frey FA, Prinz M (1978) Ultramafic inclusions from San Carlos, Arizona: petrologic and geochemical data bearing on their petrogenesis. Earth Planet Sci Lett 38:129–176

Grégoire M, Lorand JP, Cottin JY, Giret A, Mattielli N, Weis D (1997) Xenoliths evidence for a refractory oceanic mantle percolated by basanitic melts beneath the Kerguelen archipelago. Eur J Miner 9:1085–1100

Griffin WL, O'Reilly SY, Ryan CG (1998) The composition and orgin of sub-continental lithospheric mantle. In: Fei Y (ed) Mantle petrology: field observations and high-pressure experimentation. Special Publication, Geohemical Society

Griffin WL, Shee SR, Ryan CG, Win TT, Wyatt BA (1999) Harzburgite to lherzolite and back again: metasomatic processes in ultramafic xenoliths from the Wesselton kimberlite, Kimberley, South Africa. Contrib Mineral Petrol 134:232–250

Hauri EH, Shimizu N, Dieu JJ, Hart SR (1993) Evidence for hotspot-related carbonatite metasomatism in the oceanic upper mantle. Nature 365:221–227

Ianovici V, Vlad S, Borcos M, Bostinescu S (1977) Alpine porphyry copper mineralization of West Romania. Mineralium Deposita 12:307–317

Ionov DA, Hofmann AW, Shimizu N (1994) Metasomatism-induced melting in mantle xenoliths from Mongolia. J Petrol 35:753–785

Ionov DA, O'Reilly SY, Ashchepkov IV (1995a) Feldspar-bearing lherzolite xenoliths in alkali basalts from Hamar-Daban, southern Baikal region, Russia. Contrib Mineral Petrol 122:174–190

Ionov DA, Prikhod'ko VS, O'Reilly SY (1995b) Peridotite xenoliths from the Sikhote-Alin, south-eastern Siberia, Russia: trace element signatures of mantle beneath a convergent continental margin. Chem Geol 120:275–294

Ionov DA, Gregoire M, Prikhod'ko VS (1999) Feldspar-Ti-oxide metasomatism in off-cratonic continental and oceanic upper mantle. Earth Planet Sci Lett 165:37–44

Irvine TN (1967) Chromian spinel as a petrogenetic indicator. Part 2. Petrologic applications. Can J Earth Sci 4:71–103

Irving AJ (1974) Megacrysts from the newer basalts and other basaltic rocks of south-eastern Australia. Neues Jahrb Miner Abh 85:1503–1514

Irving AJ, Frey FA (1984) Trace element abundances in megacrysts and their host basalts: constraints on partition coefficients and megacrysts genesis. Geochim Cosmochim Acta 48:1201–1221

Jovanović M, Downes H, Vaselli O, Cvetković V, Prelević D, Pécskay Z (2001) Paleogene mafic alkaline volcanic rocks of East Serbia. Acta Volcanol 13(1–2):159–173

Kamenetsky VS, Crawford AJ, Meffre S (2001) Factors controlling chemistry of magmatic spinel: an empirical study of associated olivine, Cr-spinel and melt inclusions from primitive rocks. J Petrol 42(4):655–671

Karamata S, Krstić B, Dimitrijević MD, Knežević V, Dimitrijević MN, Filipović I (1994) Terranes between Adriatic and the Carpatho-Balkanian Arc. Bull Acad Serbe Sci Arts CVIII 35:47–66

Karamata S, Knežević V, Pécskay Z, Đorđević M (1997) Magmatism and metallogeny of the Ridanj-Krepoljin belt (eastern Serbia) and their correlation with northern and eastern analogues. Mineralium Deposita 32:452–458

Kelemen PB (1990) Reaction between ultramafic rock and fractionating basaltic magma. I. Phase relations, the origin of calc-alkaline magma series, and the formation of discordant dunite. J Petrol 31:51–98

Kepezhinskas PK, Defant MJ, Drummond MS (1995) Na metasomatism in the island-arc mantle by slab melt-peridotite interaction; evidence from mantle xenoliths in the North Kamchatka Arc. J Petrol 36:1505–1527

Klügel A (2001) Prolonged reactions between harzburgite xenoliths and silica-undersaturated melt: implications for dissolution and Fe–Mg interdiffusion rates of orthopyroxene. Contrib Mineral Petrol 141:1–14

Kushiro I (1976) Changes in viscosity and structure of melt of $NaAlSi_2O_6$ composition at high pressures. J Geophys Res 81:6347–6350

Lankreijer A, Mocany V, Cloetingh S (1997) Lateral variations in lithosphere strength in the Romanian Carpathians: constraints on basin evolution. In: Neubauer F et al (eds) Tectonics of the Alpine-Carpathian-Pannonian Region, II. Tectonophysics 272:269–290

Marchev P, Harkovska A, Pécskay Z, Vaselli O, Downes H (1997) Nature and age of the alkaline basaltic magmatism south-east of Krumovgrad, SE-Bulgaria. Compt Rend Acad Bulg Sci 50(4):77–80

Mason PRD, Jarvis KE, Downes H, Vannucci R (1999) Determination of incompatible trace elements in mantle clinopyroxenes by LA-ICP-MS: a comparison of analytical performance with established techniques. Geostand Newslett 23(2):157–172

McGuire AV, Mukasa SB (1997) Magmatic modification of the uppermost mantle beneath the Basin and Range to Colorado Plateau Transition Zone; Evidence from xenoliths, Wikieup, Arizona. Contrib Mineral Petrol 128:52–65

McInnes BIA, Grégoire M, Binns RA, Herzig PM, Hannington MD (2001) Hydrous metasomatism of oceanic sub-arc mantle, Lihir, Papua New Guinea: petrology and geochemistry of fluid-metasomatised mantle wedge xenoliths. Earth Planet Sci Lett 188:169–183

Menzies M (1983) Mantle ultramafic xenoliths in alkaline magmas: evidence for mantle heterogeneity modified by magmatic activity. In: Hawkesworth CJ, Norry MJ (eds) Continental basalts and mantle xenoliths. Shiva Publications, pp 92–110

Mercier JC (1979) Peridotite xenoliths and dynamics of kimberlite intrusion. In: Boyd FR, Meyer HOA (eds) The mantle sample: inclusions in kimberlites and other volcanics. Am Geophys Union Washington, pp 197–212

Mercier JC (1980) Single-pyroxene thermobarometry. Tectonophysics 70:1–37

Mercier JC, Nicolas A (1975) Textures and fabrics of upper mantle peridotites as illustrated by basalt xenoliths. J Petrol 16:454–487

Morishita T, Arai S, Green DH (2003) Evolution of low-Al orthopyroxene in the Horoman Peridotite, Japan: an unusual indicator of metasomatizing fluids. J Petrol 44(7):1237–1246

Nicolas A, Lucazeau F, Bayer R (1987) Peridotite xenoliths in Massif Central basalts: textural and geophysical evidence for asthenospheric diapirism. In: Nixon PH (ed) Mantle xenoliths. Wiley, Chichester, pp 563–574

O'Reilly SY (1989) Xenolith types, distribution and transport. In: Johnson RW (ed) Intraplate volcanism in eastern Australia and New Zealand. Cambridge University Press, Cambridge, pp 249–253

Pollack HN, Chapman DS (1977) On the regional variation of heat flow, geotherms, and lithospheric thickness. Tectonophysics 38:279–296

von Quadt A, Peytcheva I, Heinrich Ch, Frank M, Cvetković V, Banješević M (2003) Evolution of the Cretaceous magmatism in the Apuseni-Timok-Srednogorie metallogenic belt and implications for the geodynamic reconstructions: new insight from geochronology, geochemistry and isotope studies. In: Final GEODE-ABCD Workshop Programme and Abstracts, p 60

Righter K, Carmichael ISE (1993) Mega-xenocrysts in alkali olivine basalts: fragments of disrupted mantle assemblages. Am Miner 78:1230–1245

Roeder PL, Campbell IH (1985) The effect of postcumulus reactions on compositions of chrome-spinels from the Jimberlana intrusion. J Petrol 26:763–786

Sachsenhofer RF, Lankreijer A, Cloetingh S, Ebner F (1997) Subsudence analysis and quantitative basin modeling in the Styrian Basin (Pannonian Basin System, Austria). In: Neubauer F et al (eds) Tectonics of the Alpine-Carpathian-Pannonian Region, II. Tectonophysics 272:175–196

Schiano P, Clocchiatti R, Shimizu N, Weis D, Mattielli N (1994) Cogenetic silica-rich and carbonate-rich melts trapped in mantle minerals in Kerguelen ultramafic xenoliths: implications for metasomatism in the oceanic upper mantle. Earth Planet Sci Lett 123:167–178

Schiano P, Clocchiatti R, Shimizu N, Maury RC, Jochum KP, Hofmann AW (1995) Hydrous, silica-rich melts in the sub-arc mantle and their relationship with erupted arc lavas. Nature 337:595–600

Shaw CSJ (1999) Dissolution of orthopyroxene in basanitic magma between 0.4 and 2 GPa: further implications for the origin of Si-rich alkaline glass inclusions in mantle xenoliths. Contrib Mineral Petrol 135:114–132

Shaw CSJ, Eyzaguirre J (2000) Origin of megacrysts in the mafic alkaline lavas of the West Eifel volcanic field, Germany. Lithos 50:75–95

Smith DJC, Riter A (1997) Genesis and evolution of low-Al orthopyroxene in spinel-peridotite xenoliths, Grand Canyon field, Arizona, USA. Contrib Mineral Petrol 127:391–404

Streckeisen A (1973) Plutonic Rocks. Classification and nomenclature recommended by the IUGS subcommission on the sistematics of igneous rocks. Geotimes 18(10):26–30

Sun SS, McDonough WF (1989) Chemical and isotopic systematics of oceanic basalts: implications for mantle composition and processes. In: Saunders AD, Norry MJ (eds) Magmatism in ocean basins. Geol Soc Spec Publ 42:313–345

Szabó Cs, Vaselli O, Vannucci R, Bottazzi P, Ottolini L, Coradossi N, Kubovics I (1995) Ultramafic xenoliths from the Little Hungarian Plain (Western Hungary): a petrologic and geochemical study. Acta Volcanol 7(2):219–263

Szabó Cs, Bodnar R, Sobolev A (1996) Metasomatism associated with subduction-related volatile-rich silicate melt in upper mantle beneath the Nógrád-Gömör Volcanic Field, Northern Hungary/Southern Slovakia: evidence from silicate melt inclusions. Eur J Miner 8:881–899

Vannucci R, Bottazzi P, Wulff-Pedersen E, Neumann ER (1998) Partitioning of REE, Y, Sr, Zr and Ti between clinopyroxene and silicate melts in the mantle under La Palma (Canary Islands): implications for the nature of the metasomatic agents. Earth Planet Sci Lett 158:39–51

Vaselli O, Marchev P, Downes H, Coradossi N, Ingram G (1997) Ultramafic xenoliths from Chatala and Kamuka volcanoes (Northern Bulgaria). Compt Rend Acad Bulg Sci 50(4):73–76

Wells PRA (1977) Pyroxene thermometry in simple and complex systems. Contrib Mineral Petrol 62:129–139

Wilshire HG, Pike JEN (1975) Upper mantle diapirism: evidence from analogous features in alpine peridotites and ultramafic inclusions in basalt. Geology 3:467–470

Wilshire HG, Shervais JW (1975) Al-Augite and Cr-diopside ultramafic xenoliths in rocks from western United States. Phys Chem Earth 9:257–272

Witt-Eickschen G, Kramm U (1998) Evidence for the multiple stage evolution of the subcontinental lithospheric mantle beneath the Eifel (Germany) from pyroxenite and composite pyroxenite/peridotite xenoliths. Contrib Mineral Petrol 131:258–272

Wood BJ (1991) Oxygen barometry of spinel peridotites. Rev Miner 25:417–432

Wood BJ, Banno S (1973) Garnet-orthopyroxene and orthopyroxene-clinopyroxene relationship in simple and complex systems. Contrib Mineral Petrol 42:109–124

Wulff-Pedersen E, Neumann ER, Jensen BB (1996) The upper mantle under La Palma, Canary Islands: formation of Si–K–Na-rich melt and its importance as a metasomatic agent. Contrib Mineral Petrol 125:113–139

Wulff-Pedersen E, Neumann ER, Vannucci R, Bottazzi P, Ottolini L (1999) Silicic melts produced by reaction between peridotite and infiltrating basaltic melts: ion probe data on glasses and minerals in veined xenoliths from La Palma, Canary Islands. Contrib Mineral Petrol 137:59–82

Xu Y, Mercier J-CC, Menzies MA, Ross JV, Harte B, Lin C, Shi L (1996) K-rich glass-bearing wehrlite xenoliths from Yitong, Northeastern China: petrological and chemical evidence for mantle metasomatism. Contrib Mineral Petrol 125:406–420

Xu YG, Menzies MA, Bodinier JL, Bedini RM, Vroon P, Mercier JCC (1998) Melt percolation and reaction atop a plume: evidence from the pokiloblastic peridotite xenoliths from Boreé (Massif Central, France). Contrib Mineral Petrol 132:65–84

Zangana NA (1995) Geochemical variations in mantle xenoliths from Ray Pic, Massif Central, France. Unpublished PhD Thesis, University of London

Zangana NA, Downes H, Thirlwall MF, Bea F, Marriner GF (1999) Geochemical variations in peridotite xenoliths and their constituent clinopyroxenes from Ray Pic (French Massif Central): implications for the composition of the shallow lithospheric mantle. Chem Geol 153:11–35

Zinngrebe E, Foley S (1995) Metasomatism in mantle xenoliths from Gees, West Eifel, Germany: evidence from the genesis of calc-alkaline glasses and metasomatic Ca-enrichment. Contrib Mineral Petrol 122:79–96